Journal of Steroid Biochemistry and Molecular Biology 235 (2023) 106406

Contents lists available at ScienceDirect

Journal of Steroid Biochemistry and Molecular Biology

journal homepage: www.elsevier.com/locate/jsbmb

The oxidation of steroid derivatives by the CYP125A6 and CYP125A7 enzymes from *Mycobacterium marinum*

Amna Ghith, Stephen G. Bell *

Department of Chemistry, University of Adelaide, SA 5005, Australia

ARTICLE INFO

Keywords:
Metalloenzymes
Steroid metabolism
Cytochrome P450 enzymes
Mycobacteria
Cholesterol

ABSTRACT

The members of the bacterial cytochrome P450 (CYP) monooxygenase family CYP125, catalyze the oxidation of steroid derivatives including cholesterol and phytosterols, as the initial activating step in their catabolism. However, several bacterial species contain multiple genes encoding CYP125 enzymes and other CYP enzymes which catalyze cholesterol/cholest-4-en-3-one hydroxylation. An important question is why these bacterium have more than one enzyme with overlapping substrate ranges capable of catalyzing the terminal oxidation of the alkyl chain of these sterols. To further understand the role of these enzymes we investigated CYP125A6 and CYP125A7 from *Mycobacterium marinum* with various cholesterol analogues. These have modifications on the A and B rings of the steroid and we assessed the substrate binding and catalytic activity of these with each enzyme. CYP125A7 gave similar results to those reported for the CYP125A1 enzyme from *M. tuberculosis*. Differences in the substrate binding and catalytic activity with the cholesterol analogues were observed with CYP125A6. For example, while cholesteryl sulfate could bind to both enzymes it was only oxidized by CYP125A6 and not by CYP125A7. CYP125A6 generated higher levels of metabolites with the majority of C-3 and C-7 substituted cholesterol analogues such 7-ketocholesterol. However, 5α-cholestan-3β-ol was only oxidized by CYP125A7 enzyme. The cholest-4-en-3-one and 7-ketocholesterol-bound forms of the CYP125A6 and CYP125A7 enzymes were modelled using AlphaFold. The structural models highlighted differences in the binding modes of the steroid derivatives within the same enzyme. Significant changes in the binding mode of the steroids between these CYP125 enzymes and other bacterial cholesterol oxidizing enzymes, CYP142A3 and CYP124A1, were also seen. Despite this, all these models predicted the selectivity for terminal methyl hydroxylation, in agreement with the experimental data.

1. Introduction

Tuberculosis (TB) remains one of the leading causes of death from bacterial infection. *Mycobacterium tuberculosis* infects one-third of the human population and is responsible for nearly 1.5 million deaths annually (WHO, 2021) [1]. The major contributor to these high infection rates is the ability of *M. tuberculosis* to persist within the host as a latent (asymptomatic) infection, and once the immune system is compromised, it is reactivated [2]. This pathogen is characterized by its innate resistance to antibiotics, due to its extremely slow growth rate and the complex lipid composition of its cell wall. The emergence of multiple-drug-resistant (MDR) and extremely drug-resistant (XDR) strains of this bacterium has made treatment more difficult, and as a result, tuberculosis is considered an existential threat to public health [3].

The infectivity and persistence of *M. tuberculosis* are linked to its ability to use host cell cholesterol. *M. tuberculosis* cannot synthesize steroids *de novo*, but it can successively utilize host-derived lipids such as cholesterol in the active phase of infection which is known as a defining characteristic of this pathogen [4]. *M. tuberculosis* utilizes cholesterol and other nutrients, to generate end products within the bacterium which facilitate its pathogenesis. It has been reported that *M. tuberculosis*

Abbreviations: BSTFA, N,O-bis(trimethylsilyl)trifluoroacetamide; CYP or P450, cytochrome P450 enzyme; DMSO, dimethyl sulfoxide; DTT, dithiothreitol; HβCD, (2-hydroxypropyl)-β-cyclodextrin; IPTG, isopropyl β-D-1-thiogalactopyranoside; LB, lysogeny broth (also known as Luria or Lennox Broth), MDR, multi drug-resistant; MeCN, acetonitrile; NTB, nontuberculous mycobacteria; NADPH, reduced nicotinamide adenine dinucleotide (phosphate); SOC, Super Optimal broth with Catabolite repression; Tris, tris(hydroxymethyl)aminomethane; WT, wild-type; XDR, extensively drug-resistant.

* Corresponding author.
E-mail address: stephen.bell@adelaide.edu.au (S.G. Bell).

https://doi.org/10.1016/j.jsbmb.2023.106406
Received 16 August 2023; Received in revised form 24 September 2023; Accepted 30 September 2023
Available online 2 October 2023

switches its metabolic pathways to lipids rather than carbohydrates during infection [5]. Therefore, cholesterol has a pivotal role during both chronic and latent phases of infection and is an important source of carbon and energy. The steroid is catabolized by a set of enzymes to fuel central metabolic pathways to facilitate the bacterium's persistence [6]. *M. tuberculosis* has a thick cell wall structure made up of lipid- and carbohydrate-rich layers that serve as a permeability barrier against drugs and this enhances the survival of the pathogen [7]. One of the roles of the cholesterol degradation pathway is to incorporate the cholesterol side chain carbon atoms into components of the cell wall. Cholesterol breakdown results in the release of propionyl-CoA, which is biosynthetically used to synthesize methyl-branched, polyketide virulence lipids, that make up the bacterial cell wall [8,9]. By contributing to the pool of propionyl-CoA part of the cholesterol molecule are incorporated into lipid virulence factors such as methyl-branched phthiocerol dimycocerosates (PDIM) [10,11].

While *M. tuberculosis* remains the most notorious mycobacterial species, there are other nontuberculous mycobacteria (NTB) that can cause disease. For example, *Mycobacterium ulcerans* and *Mycobacterium leprae,* cause Buruli ulcer and leprosy, respectively [12,13]. In addition, *Mycobacterium avium* lung infections are associated with poor clinical outcomes and are on the rise [14]. Another example of an NTB, or an atypical mycobacteria is *Mycobacterium marinum*. This species can cause outbreaks of a tuberculosis-like infection in fish and skin infections in humans [15]. Humans are the only known reservoir for *M. tuberculosis*, *M. ulcerans* and *M. leprae* while *M. marinum* can survive outside the host. *M. marinum* is hypothesized to resemble the most recent common ancestor of *M. tuberculosis* and *M. ulcerans*, with which it shares a high degree of sequence similarity (85% and 97%, respectively) [16]. *M. marinum* shares 3000 orthologous proteins with *M. tuberculosis* [16], and has been used as a model organism to plot the evolutionary pathway of other mycobacterium pathogens and to facilitate the understanding of how *M. tuberculosis* causes disease [17]. It is significant that many of the genes encoding for the mycobacterial cell wall biosynthesis are shared by *M. marinum, M. ulcerans,* and *M. tuberculosis*. The similar cell wall structures of each bacterium are constructed by enzymes that have no human orthologue making them attractive drug targets. [7,18–20].

Sequencing of the *M. tuberculosis* genome revealed that roughly 10% of its genes were involved in lipid biosynthesis and metabolism [21,22]. Similar steroid catabolism pathways, and the enzyme encoding genes within them, are also found in other actinobacteria such as *Rhodococcus jostii*, as well as the non-pathogenic mycobacterial species *M. smegmatis* and *M. marinum* [23,24]. Steroid catabolism is important as it is a readily available carbon and energy source from plant and animal organic matter. Bacterial steroid catabolism is initiated by heme-thiolate monooxygenase cytochrome P450 (CYP) enzymes. Cholesterol utilization is initiated by the uptake of the steroid into the bacterial cell, which can be oxidized to cholest-4-en-3-one by a mycobacterial 3β-hydroxysterol dehydrogenase (3β-HSD) [25]. Next, the side chain degradation of the steroid is initiated by CYP125 and CYP142 enzymes. They oxidize the terminal methyl (C-26) of either steroid to a carboxylic acid via an initial ω-hydroxylation step (Scheme 1) [26–28]. The CYP125A1 enzyme of *M. tuberculosis* is also reported to catalyze a C-C bond cleavage reaction with the aldehyde intermediate [29]. Further steps in the process result in β-oxidation of the side-chain which gives two equivalents of propionylCoA and 4-androstenedione, the latter of which can undergo further degradation releasing two more equivalents of propionylCoA [10]. These four propionylCoA fragments are incorporated into cellular lipids and virulence factors. Cholesterol degradation appears to be a major source of this key metabolite *in vivo* [30,31].

There are 20 cytochrome P450 enzymes enzyme encoding genes in *M. tuberculosis* several of which are necessary for steroid catabolism and for cell function or infectivity [32,33]. *M. marinum*, has a higher number of CYP genes (47) compared to its close relative the human pathogen *M. ulcerans*, which has 24 genes. The lower number of CYPs in *M. ulcerans* and *M. tuberculosis* is thought to be caused by reductive evolution as they specialized towards pathogenicity [12,16,34,35].

There are at least three cholesterol metabolizing cytochrome P450 isoforms in *M. tuberculosis*; CYP125A1, CYP142A1 and CYP124A1 that can initiate the oxidation of steroid alkyl side chain, with the CYP125 enzyme proposed to be the most important, followed by the CYP142 enzyme (Scheme 1) [10,33,36]. The CYP124A1 enzymes can also oxidize branched fatty acid lipids and vitamin D3 derivatives [37,38]. Several CYP125 enzymes from other actinobacteria and mycobacteria which all catalyze the oxidation of cholesterol at C-26 have also been identified. These include CYP125A3 and CYP125A4 from *M. smegmatis*, CYP125A6 and CYP125A7 from *M. marinum* [39,40]. Recently it was demonstrated that the CYP125 enzymes are capable of oxidizing the phytosterols, sitosterol and campesterol. In contrast, the CYP142 and CYP124 enzymes had much lower activity for sitosterol compared to

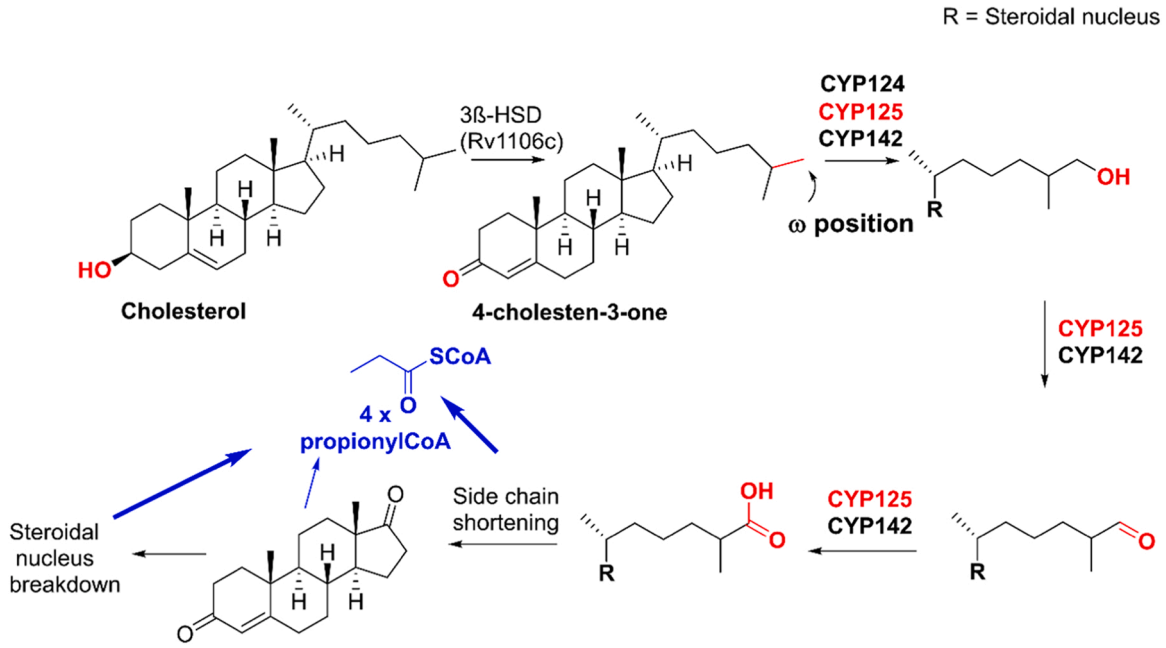

Scheme 1. Steroid nucleus degradation initiated by cytochrome P450 (CYP125, CYP142 and CYP124) enzymes.

cholesterol [41].

An important question is why do some bacterium have two or more copies of genes encoding CYP125 family enzymes [24], when the CYP142 and CYP124 family enzymes can also catalyze the oxidation of the same, and related steroid substrates to yield ω-oxidation metabolites. Another noteworthy observation is that in *M. tuberculosis* the double knockout of both the CYP125A1 and CYP142A1 enzyme genes prevents its growth on cholesterol. However, double knockout of CYP125A3 and CYP142A2 in *M. smegmatis* does not due to the presence of the additional CYP125A4 enzyme [40]. The two *M. smegmatis* CYP125 enzymes, CYP125A3 and CYP125A4, share 78% and 71% amino acid sequence identity to CYP125A1, respectively. The sequence identities of the CYP125A6 (75%) and CYP125A7 (90%) enzymes of *M. marinum* show that the latter is more similar to CYP125A1 (Fig. S1 and Table S1) [38]. CYP125A6 and CYP125A7 share 76% sequence identity (Fig. S1). CYP125A3 from *M. smegmatis* is more closely related in amino acid sequence to CYP125A7 than CYP125A6 (78% versus 69%), while CYP125A4 from *M. smegmatis* is closer to CYP125A6 (82% compared to 71% for CYP125A7). Small changes in sequence within or close to the active site can significantly alter substrate binding between different CYP enzymes [42]. For example, although CYP125A4 from *M. smegmatis* can oxidize cholesterol it is reported to have a higher activity for the oxidation of 7α-hydroxycholesterol. This is proposed to be due to changes in an aromatic residue close to the active site of the enzyme where the C-7 carbon is located. In the CYP125A1 enzyme it is a phenylalanine (Phe 100), but in CYP125A3 it is a tryptophan (Trp 83), a tyrosine in CYP125A4 (Tyr 87). It is a tyrosine in CYP125A6 (Tyr 91) and a phenylalanine in CYP125A7 (Phe 84) from *M. marinum* [40].

Here we further investigate the substrate specificity of the two CYP125 enzymes (CYP125A6 and CYP125A7) from *M. marinum* with different cholesterol analogues (Fig. 1) and assess whether these enzymes can oxidize them. The different cholesterol and cholest-4-en-3-one analogues were chosen to determine the importance of different substitutions on the A and B rings of cholesterol (Fig. 1). We focus on the C-3 substituent (e.g. cholesteryl acetate and 5α-cholestane), the presence and location of a double bond (e.g. 5α-cholestan-3-one, the diastereomers of 5-cholestan-3-ol, and cholesterol-5α,6α-epoxide), and the effect of modifications at C-7 (e.g. 7-ketocholesterol and 7-dehydrocholesterol; Fig. 1) [40,43]. Some of the oxysterol analogues tested are products of cholesterol autoxidation or enzymatic oxidation [44,45] and can be found at elevated concentrations during infection. In addition, those that do not have an A/B ring alkene are often found in the environment alongside cholesterol as components of organic matter e.g., the 5-cholestan-3-ols [46,47]. Docking studies were performed to assess the potential binding mode and to characterize the interactions of selected analogues (cholest-4-en-3-one and 7-ketocholesterol) within the active site of both CYP125A6 and CYP125A7 and were compared to the cholest-4-en-3-one-bound structure of CYP125A1 (PDB 2X5W) [48].

2. Materials and methods

2.1. General

Steroid substrates, including cholesterol and its derivatives, were

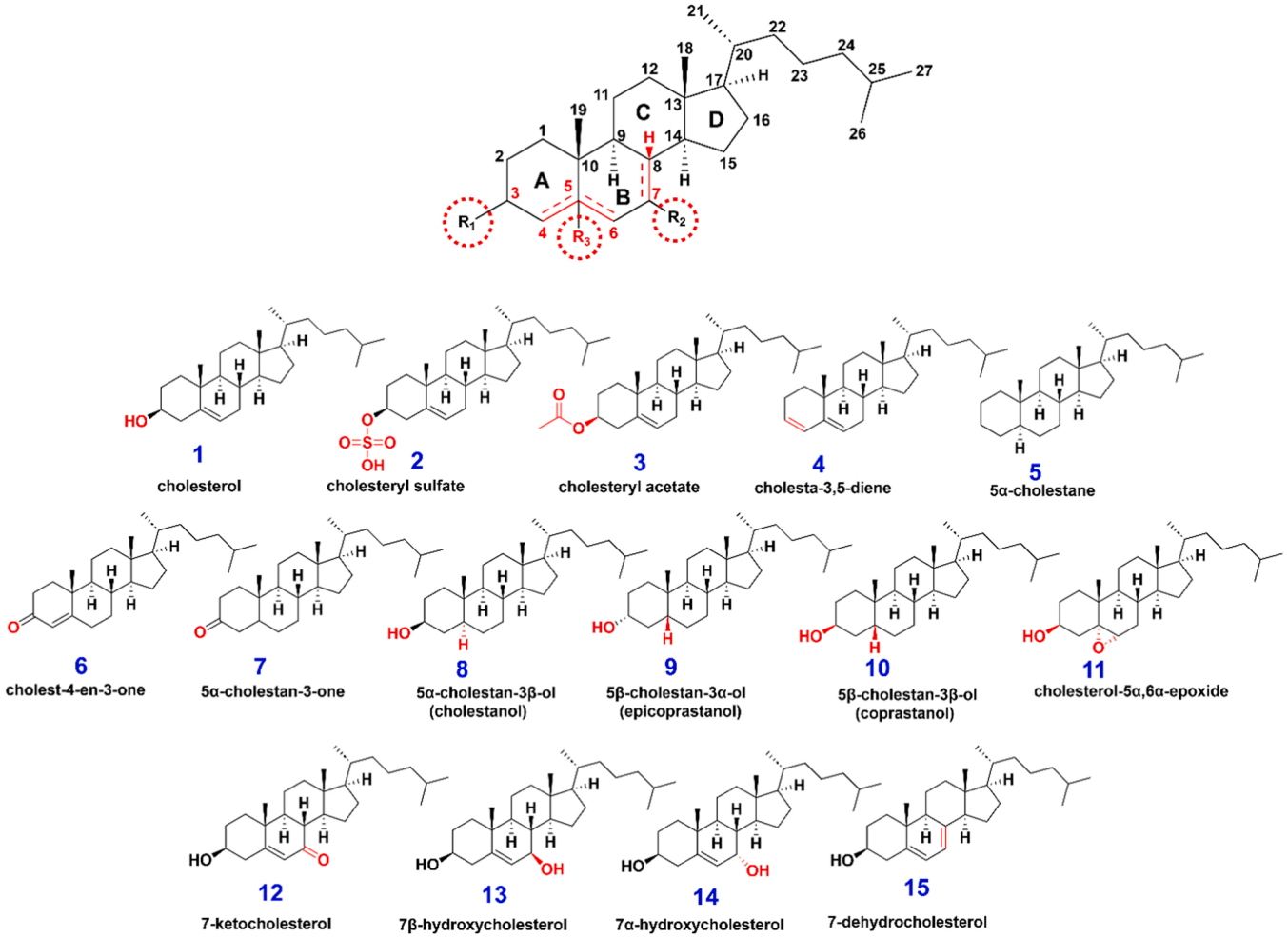

Fig. 1. Chemical structures of the cholesterol analogues **1–15** investigated in this work.

purchased from Biosynth (UK) or Sigma-Aldrich (Merck, Australia). Ferredoxin-NADP+ reductase (*S. oleracea*), catalase (bovine), and other general reagents, organic solvents, and derivatization agents were purchased from Sigma-Aldrich (Australia), Biosynth (UK), or ChemSupply (Australia). Isopropyl-β-D thiogalactopyranoside (IPTG), Kanamycin, DTT, and buffer components were obtained from Astral Scientific (Australia). NADPH was from Applichem (Australia), and glucose-6-phosphate and glucose-6-phosphate dehydrogenase were from Roche (Germany). The media for cell growth and maintenance (LB, SOC, and trace elements) were prepared as reported previously [39]. Kanamycin was added to a working concentration of 30 μg mL^{-1}. UV–vis absorbance spectra were recorded on an Agilent Cary 60 spectrophotometer at 30 ± 0.5 °C.

2.2. Recombinant protein expression and purification

2.2.1. Production and purification of cytochrome P450 enzymes

The *M. marinum* CYP125A6 and CYP125A7 genes from the genomic DNA were amplified and cloned into pET26, as reported previously [49]. Both CYP125A6 and CYP125A7 proteins used in this study, were generated by transforming the respective vector into *E. coli* BL21 (DE3) cells. The growth and induction conditions used for protein production of each CYP enzyme were the same as those used and reported previously [39,50].

The CYP125 enzymes were purified by DEAE ion exchange chromatography, desalted using Sephadex G-25 and then further purified by Source Q ion-exchange chromatography step [39]. A gradient elution (100–400 mM KCl in 50 mM Tris buffer, pH 7.4 – Tris buffer) was performed. Fractions containing the cytochrome P450 were pooled and concentrated. A final desalting step was implemented using Tris buffer as an eluent. The purity of the proteins was assessed by their UV–vis absorbance at 412 nm which is the isosbestic point between the low-spin and high-spin P450 heme states. ($A_{412}/A_{280} > 0.6$–0.7 for both CYP125 enzymes). The purified proteins were stored in glycerol (50% v/v at −20 °C). A 5 mL PD-10 column (GE Healthcare) in 50 mM Tris buffer pH 7.4 was used to remove the glycerol prior to use in subsequent experiments. The extinction coefficient (ε_{412} = 97 mM^{-1} cm^{-1}) was used to calculate the concentration of CYP125A6 and CYP125A7 enzymes [41].

2.2.2. Production and purification of ferredoxin from Spinacia oleracea

A plasmid containing a codon optimized gene encoding the ferredoxin from *Spinacia oleracea*, was transformed in *E. coli* BL21 (DE3) competent cells. The transformed cells were then plated on LB agar plate containing kanamycin (30 mg L^{-1}) incubated at 37 °C overnight. Single colonies of the bacteria were introduced into four 500 mL volumes of LB broth media containing kanamycin (30 mg L^{-1}) of a total growth volume of 2 L. The cells were grown at 37 °C at 100 rpm for approximately 8 hrs then they were cooled by reducing the temperature to 18 °C. Subsequently, 2% v/v EtOH and 0.02% v/v benzyl alcohol were added. After incubation for 30 min at 18 °C, 50 μM IPTG (isopropyl β-D-1-thiogalactopyranoside) was added to induce the expression and production of the spinach ferredoxin protein. The cultures were incubated for almost 48 h at 18 °C and 80 rpm. The cultures were centrifuged (5000 *g*, 10 min, 4 °C) and the cell pellet, was stored at − 20 °C. The cells were re-suspended in 150 mL of 50 mM Tris buffer pH 7.4 and the cells were lysed by sonication (22 cycles of 10:50 s on/off, 70% amplitude, 19 mm probe, Sonics Vibra-Cell). The cell debris was removed by centrifugation (18,000 rpm for 10 min at 4 °C). Then the protein was purified by DEAE ion exchange chromatography, using a gradient elution of (100–400 mM KCl in Tris buffer). Fractions containing the ferredoxin protein were concentrated. The salt was removed using a Sephadex G-25 medium grain size-exclusion column (GE Healthcare), and 50 mM Tris buffer, pH 7.4 was used as the eluent. The final step involves further purification by Source Q ion-exchange chromatography step using an AKTA protein purification system [39]. A gradient elution (200–500 mM KCl in Tris buffer) was performed. Fractions containing the purified protein were concentrated, then it was stored in glycerol (50% v/v at −20 °C). The extinction coefficient (9400 M^{-1} cm^{-1} at 420 nm) was used to calculate the concentration of spinach ferredoxin from previously reported methods [51].

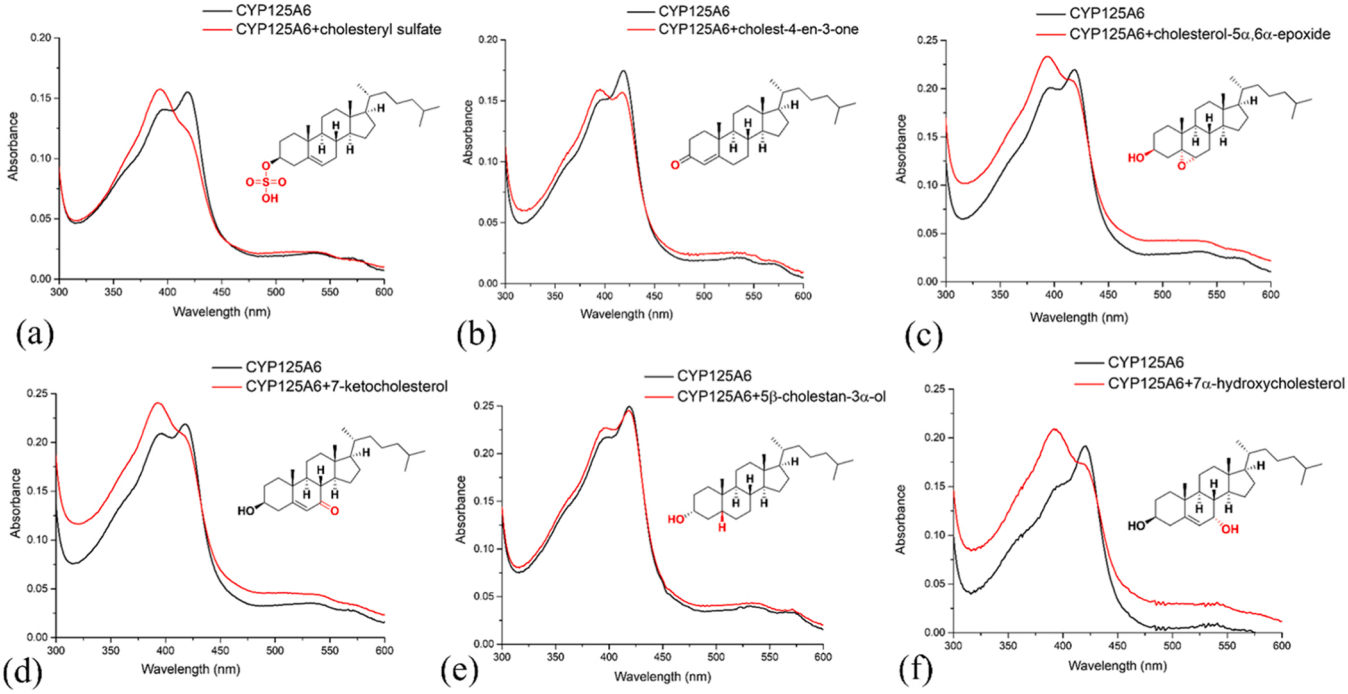

Fig. 2. The UV–vis absorbance spectra CYP125A6 after the addition of (a) cholesteryl sulfate, (b) cholest-4-en-3-one, (c) cholesterol-5α,6α-epoxide and (d) 7-ketocholesterol, (e) 5β-cholestan-3α-ol, (f) 7α-hydroxycholesterol. In black is the UV–vis spectrum of the substrate-free enzyme and in red the UV–vis absorbance spectrum of the enzyme after the addition of the substrate.

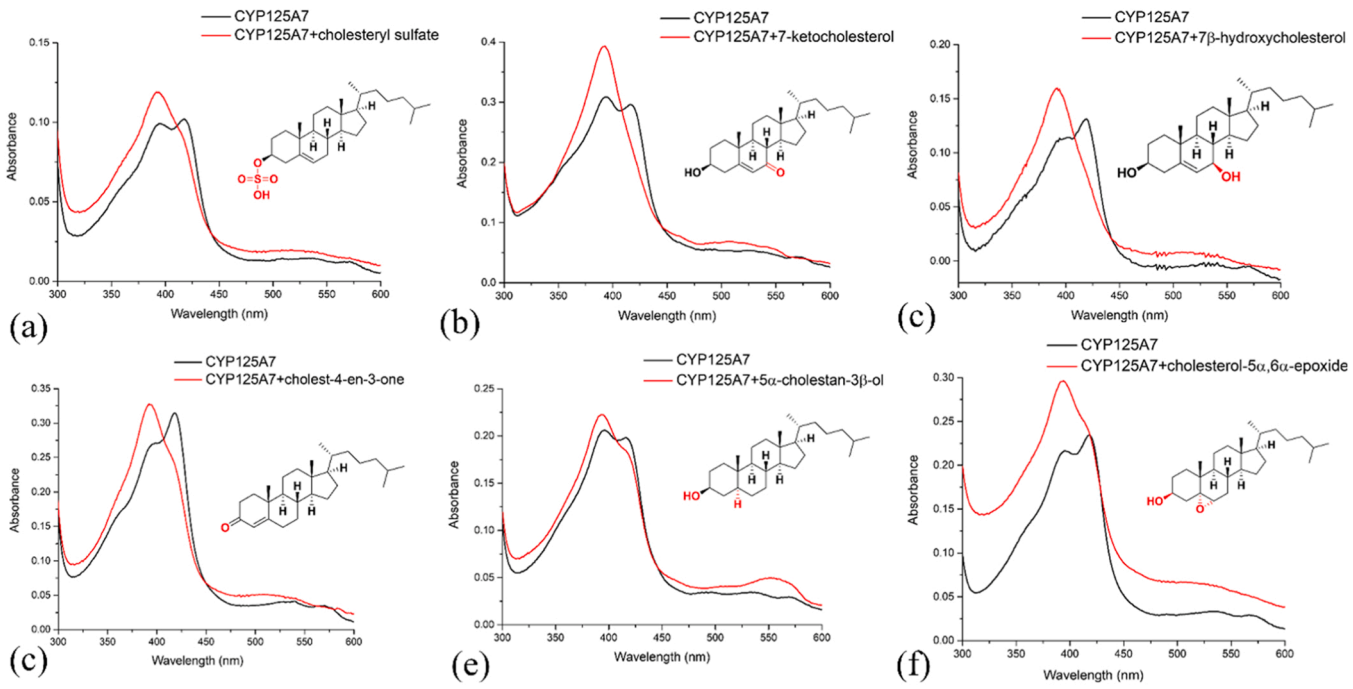

Fig. 3. The UV–vis absorbance spectra CYP125A7 after the addition of (a) cholesteryl sulfate, (b) 7-ketocholesterol, (c) 7β-hydroxycholesterol, (d) cholest-4-en-3-one, (e) 5α-cholestan-3β-ol and (f) cholesterol-5α,6α-epoxide. In black is the UV–vis spectrum of the substrate-free enzyme and in red the UV–vis absorbance spectrum of the enzyme after the addition of the substrate.

Table 1
Substrate binding analysis and the levels of product formation for the cholesterol analogues with CYP125A6, and CYP125A7. The proportion of high-spin ferric heme is expressed as a percentage (± 5%).

Substrate	Substituents				CYP125A6 Spin state Product Resting State 30%		CYP125A7 Spin state Product Resting State 45%	
	C3	C5	C7	= alkene				
cholesterol		-	-	5/6	+ 15%	✓✓✓ OH/COOH*	+ 30%	✓✓✓ OH
cholesteryl sulfate		-	-	5/6	+ 45%	✓✓ OH	+ 40%	np
cholesteryl acetate		-	-	5/6	+ 10%	np	+ 10%	np
cholesta-3,5-diene	-	-	-	3/4 & 5/6	+ 5%	np	NS	np
5α-cholestane	-	-	-	-	NS	np	NS	np
cholest-4-en-3-one		-	-	4/5	+ 20%	✓✓ OH	+ 45%	✓ OH/COOH*
5α-cholestan-3-one		-	-	-	NS	np	NS	np
5α-cholestan-3β-ol			-	-	+ 5%	np	+ 15%	✓✓ OH
5β-cholestan-3α-ol			-	-	+ 10%	✓✓ OH/COOH*	+ 15%	✓ OH/COOH*
5β-cholestan-3β-ol			-	-	< 5%	✓ OH/COOH*	+ 5%	✓✓ OH/COOH
cholesterol-5α,6α-epoxide			-	-	+ 30%	✓✓ OH/COOH*	+ 45%	✓✓ OH
7-ketocholesterol		-		5/6	+ 40%	✓✓ OH	+ 50%	✓ OH
7β-hydroxycholesterol		-		5/6	+ 25%	✓✓ OH	+ 50%	✓ OH/COOH*
7α-hydroxycholesterol		-		5/6	+ 45%	✓✓ OH	+ 25%	✓✓ OH
7-dehydrocholesterol		-	-	5/6 & 7/8	+ 5%	✓ OH	+ 20%	✓ OH

NS: No shift. np: no product. ✓ low level of metabolite formation; ✓✓ moderate level of metabolite formation; ✓✓✓ high level of metabolite formation; OH alcohol metabolite detected; COOH acid metabolite detected. * low level of the COOH acid metabolite is detected.

2.3. Substrate binding assays

For substrate binding assays, the purified CYP125 enzyme was diluted to ~1–3 μM in 50 mM Tris pH 7.4, to a volume of 600 μL, followed by the addition of the steroid substrates. Substrate stocks were made to a concentration of 1–10 mM in 50 mM Tris pH 7.4, in 10% (2-hydroxypropyl)-β-cyclodextrin (HβCD Sigma-Aldrich). The absorbance between 600 nm and 250 nm was recorded using a UV–visible spectrophotometer until no further spectral change was observed. The high-spin percentage (± 5%) was estimated by comparison to a set of spectra, as described previously [52].

2.4. Enzyme catalyzed oxidations

The cytochrome P450 enzymes (2 μM) were incubated for 2 min with 0.1 mM of the substrate, the reactions were initiated by addition of an NADPH regeneration system consisting of 1 mM NADPH, 4 μM spinach ferredoxin, 0.2 units mL^{-1} spinach ferredoxin-$NADP^+$ reductase, 0.1 mg mL^{-1} bovine liver catalase, 0.7 units mL^{-1} glucose-6-phosphate dehydrogenase, and 5 mM glucose-6-phosphate.

2.5. Gas chromatography-mass spectrometry analysis

After the enzymatic reactions were completed, octanoic acid (10 μL from 10 mM stock) was added to all the turnover reactions as an internal standard, and the reactions were extracted three times with 400 μL of EtOAc. The combined organic extracts were dried with $MgSO_4$, followed by evaporating the solvent under N_2 gas. Anhydrous MeCN (150 μL) was used to dissolve the residue and the samples were derivatized with 15 μL of (BSTFA+TMCS, 99:1) (Supelco, USA) for 2 h at 37 °C. These samples were analyzed by GC-MS using a Shimadzu GC-2010 equipped with a QP2010S GC-MS detector. The injection port temperature was 300 °C. The column (DB5ms, 30 mm × 0.25 mm×0.25 μm) was held at 70 °C for 1 min, followed by increasing the temperature to 280 °C at a rate of 15 °C min^{-1} and held at 280 °C for 1 min and finally the temperature was increased to 300 °C at a rate of 15 °C min^{-1} and held for 10 min

2.6. Molecular docking studies

Docking experiments were performed in ICM-Pro software version 3.9–3a (Molsoft L.L.C., San Diego, CA, USA) using the small molecule docking module. The X-ray crystal structure of CYP125A1 bound to cholest-4-en-3-one was obtained from the Protein Data Bank (PDB 2X5W) while the structures of CYP125A6 and CYP125A7 were from the AlphaFold Protein Structure Database [53,54]. Formal charges were assigned; protonation states of histidines were adjusted, and hydrogens, histidine, glutamine, and asparagine were optimized using the protein preparation procedure implemented in ICM [55]. If required, the ligand (cholest-4-en-3-one) in CYP125A1 was removed from the active site before docking. The receptor pocket was defined by residues with at least one non-hydrogen atom within a 4.0 Å cut-off distance from the cholest-4-en-3-one ligand. The receptor box was resized to cover this region, defined by two opposing corners with x, y, z coordinates. The proteins were energy minimized, and the molecules were manually docked into the binding site and scored based on the ICM scoring function (GBSA/MM-type scoring function) set to 10 to identify the most favourable binding conformation and side-chain interactions [56].

3. Results and discussion

3.1. Substrate binding

When assessing substrate binding to CYP125 enzymes it is important to note that they are unusual compared to the majority of cytochrome P450 enzymes in that their UV–vis absorbance spectrum shows the presence of both the high- and low-spin ferric species. CYP125A1 from *M. tuberculosis* is approximately 80–90% high-spin in its resting state [48,57]. The UV–vis absorbance spectra of the resting state of the CYP125A6 and CYP125A7 enzymes had lower high spin-character showing that CYP125A6 is ~30–45% high-spin, whereas CYP125A7 is ~35–50% high-spin (Fig. 2, Fig. 3 and Table 1) [39]. This can make the assessment and comparison of substrate binding of closely related ligands across these different enzymes more challenging. In the results below, we focus on the substrates that demonstrated large changes compared to the resting state or significant differences compared to those induced by cholesterol.

The addition of cholesterol to the CYP125A6 enzyme caused an approximate + 15% increase in the amount of the high-spin ferric species. The change observed with CYP125A7 was greater (+30%) which is indicative of an increased displacement of the sixth aqua heme ligand by the ligand (Fig. S2 and S3) [39]. The addition of cholest-4-en-3-one to CYP125A6 resulted results in a similar shift to the high-spin ferric state (+20%) as with cholesterol while the change induced in the CYP125A7 enzyme was greater (+45%) than that observed with cholesterol and with CYP125A6 (Table 1, Fig. S2 and S3).

For the analogues that modified the C-3 β-hydroxyl substituent of

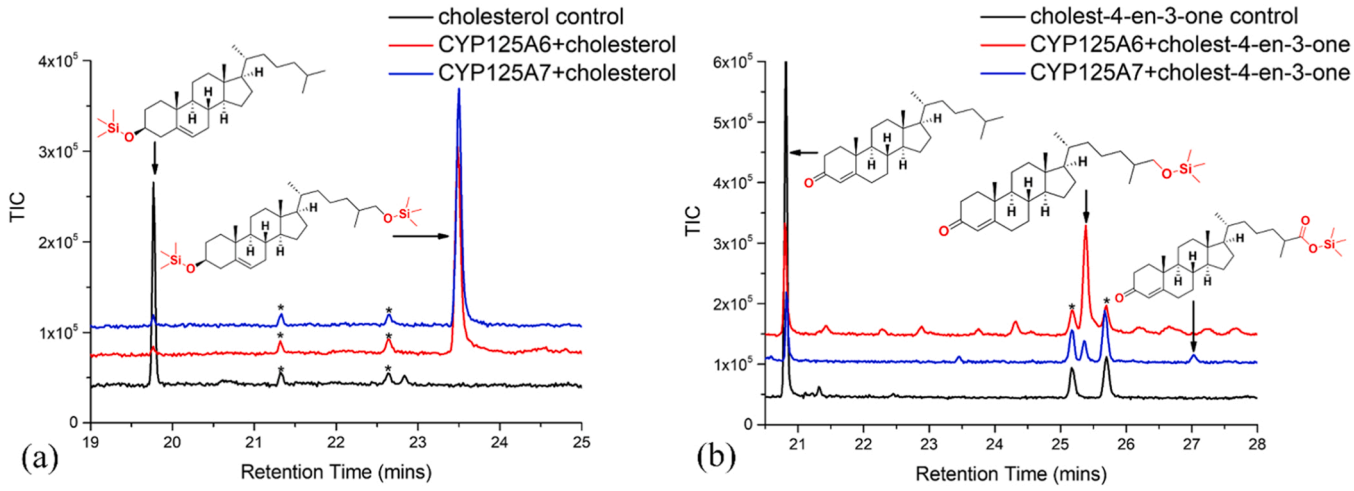

Fig. 4. The GC-MS analysis of the oxidation of (a) cholesterol and (b) cholest-4-en-3-one by the CYP125A6 (red) and CYP125A7 (blue) enzymes. A substrate control (black) is included and impurity peaks (present in substrate controls and turnover reactions) are marked with an asterisk. All samples were derivatized with BSTFA/TMSCl prior GC-MS analysis (see SI for mass spectra).

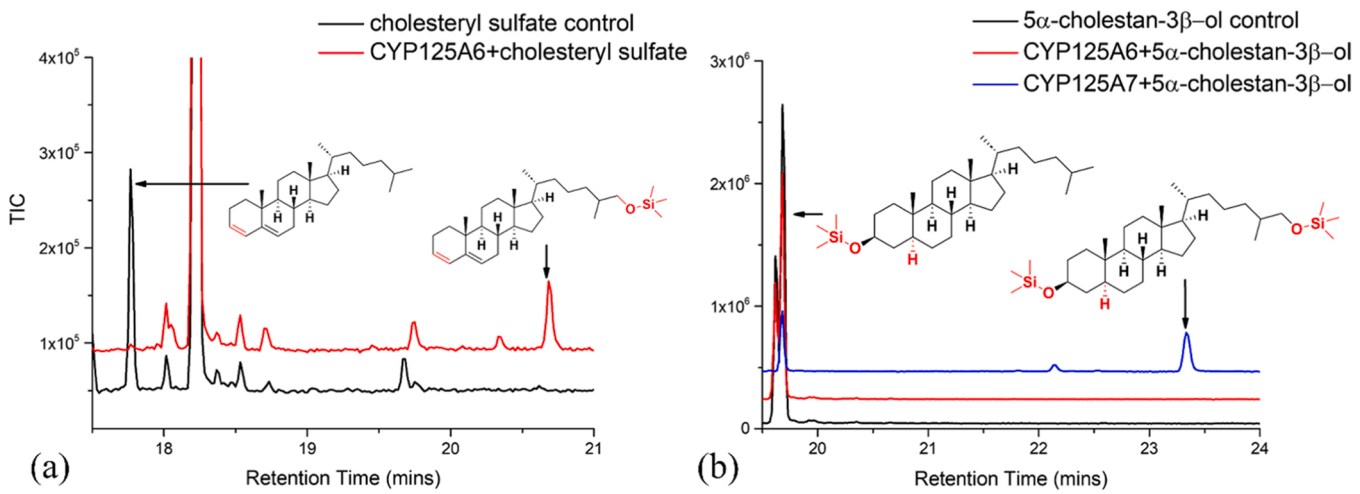

Fig. 5. The GC-MS analysis of the oxidation of (a) cholesteryl sulfate and (b) 5α-cholestan-3β-ol by the CYP125A6 (red) and CYP125A7 (blue) enzymes. The substrate control is shown in (black). All samples were derivatized with BSTFA/TMSCl prior GC-MS analysis (See Fig. S4 for CYP125A7 with cholesteryl sulfate and see SI for mass spectra).

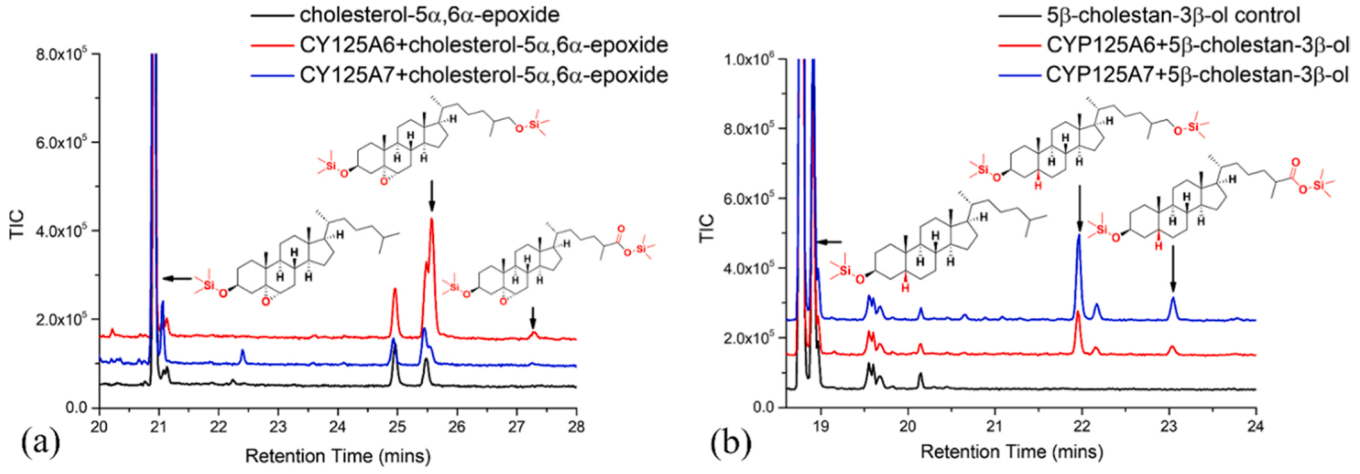

Fig. 6. The GC-MS analysis of the oxidation of (a) cholesterol-5α,6α-epoxide and (b) 5β-cholestan-3β-ol by the CYP125A6 (red) and CYP125A7 (blue) enzymes. The substrate control is shown in (black). All samples were derivatized with BSTFA/TMSCl prior GC-MS analysis (see SI for mass spectra).

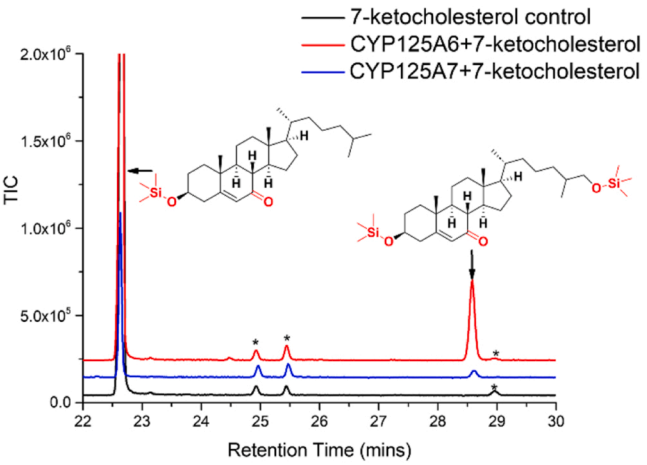

Fig. 7. The GC-MS analysis of 7-ketocholesterol by CYP125A6 (red) and CYP125A7 (blue). Also shown is a substrate control (black). Impurity peaks (present in substrate controls and turnover reactions) are marked with an asterisk. All samples were derivatized with BSTFA/TMSCl-before GC-MS analysis (see SI for further details and mass spectra).

cholesterol the majority resulted in a significantly lower, or in no discernible change, in the UV–vis absorbance spectrum of either CYP125A6 or CYP125A7 when compared to cholesterol. For example, cholesteryl acetate generated a small change (~10%) in the UV–vis spectrum with both enzymes and cholesta-3,5-diene, 5α-cholestane did not appreciably shift the Soret band of either (Fig. S2, Fig. S3 and Table 1). Cholesteryl sulfate was the exception and resulted in a larger shift to the high-spin ferric species for both enzymes when compared to cholesterol (Fig. 2 and Fig. 3; Table 1).

Removing the double bond of cholesterol or cholest-4-en-3-one also diminished the magnitude of the observed change in the UV–vis absorbance spectrum. 5α-Cholestan-3-one and 5β-cholestan-3β-ol (coprastanol) did not induce any significant shifts with either enzyme (Fig. S2 and S3, Table 1). Addition of 5β-cholestan-3α-ol (epi-coprastanol) caused a small change (≤15%) with both CYP125A6 and CYP125A7 (Fig. 2 and Fig. S3). 5α-Cholestan-3β-ol (cholestanol), which has a *trans*-decalin arrangement of the A and B steroid rings, shifted the UV–vis absorbance spectrum of both enzymes, with that of CYP125A7 (+15%) being slightly greater than that (+5%) of CYP125A6 (Fig. 3 and Fig. S2). In contrast, the addition of cholesterol-5α,6α-epoxide resulted in greater shifts to the high-spin form in both enzymes (30–45%, Fig. 2, Fig. 3 and Table 1). As with cholesteryl sulfate the magnitude of the shift

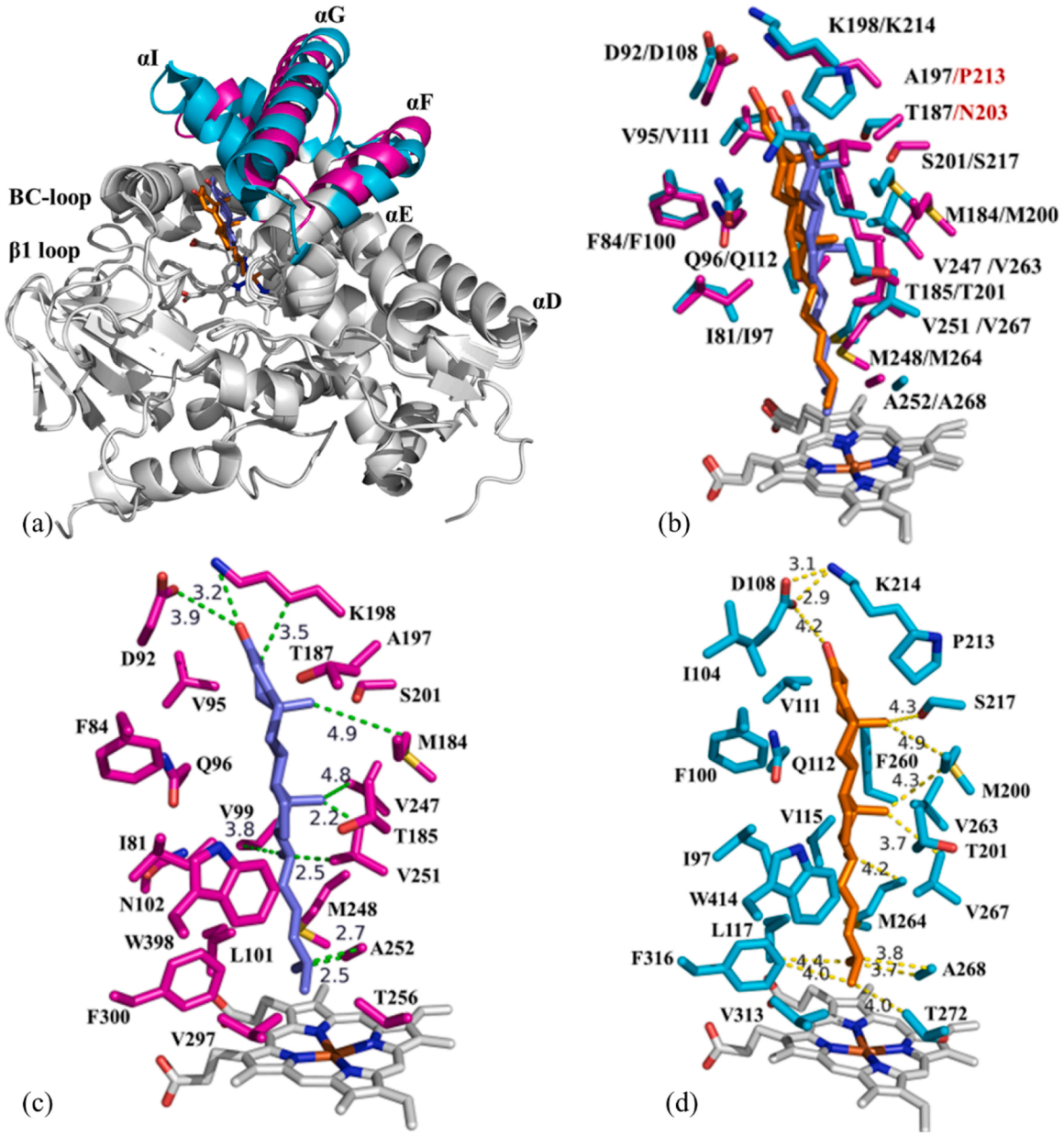

Fig. 8. (a) The superimposed structures of cholest-4-en-3-one-bound CYP125A1 (grey, highlights in teal; PDB code 2X5W) and cholest-4-en-3-one-bound CYP125A7 (grey, highlights in magenta; downloaded from AlphaFold). (b) Superimposed structures of the active sites of cholest-4-en-3-one-bound CYP125A1 (teal) and cholest-4-en-3-one-bound CYP125A7 (magenta). (c) The active site of the cholest-4-en-3-one-bound CYP125A7 with amino acids within 5 Å of ligand (d) The active site of the cholest-4-en-3-one-bound CYP125A1 (PDB 2X5W) with amino acids within 5 Å of ligand. The cholest-4-en-3-one substrate is shown in orange for CYP125A1, and in purple for CYP125A7. The conserved residues in both are labelled in black and CYP125 residues are in red.

was greater with CYP125A7 than CYP125A6 (Fig. 2, Fig. 3, and Table 1).

Of the cholesterol analogues, which were modified at C-7, 7β-hydroxycholesterol and 7-ketocholesterol resulted in a large shift (+50%) high-spin ferric heme with CYP125A7 (Fig. 3). Whereas, the addition of 7α-hydroxycholesterol and 7-dehydrocholesterol, to the CYP125A7 enzyme resulted in significant but lower shifts (+20–25%; Fig. S3). With CYP125A6, 7-ketocholesterol and 7α-hydroxycholesterol resulted in the largest shifts to the high-spin ferric state (+40–45%) which were greater in magnitude to those of cholest-4-en-3-one (Fig. 2, Fig. S2 and Table 1). 7β-hydroxycholesterol resulted in a higher shift (+25%) comparable to that of cholesterol (Fig. S2) while the change in the UV–vis absorbance spectrum after adding 7-dehydrocholesterol was observable but lower (+5%) than for the other C-7 modified cholesterol analogues (Fig. S2).

In summary, compounds that lack the substitution at C-3, such as cholesta-3,5-diene, or that changed the C-3 group to a more hydrophobic moiety e.g., cholesteryl acetate, did not induce large spectral changes with either CYP125A6 and CYP125A7 enzymes highlighting the importance of the substituent at this position. Cholesteryl sulfate, cholesterol-5α,6α-epoxide and 7-ketocholesterol, resulted in a greater change in the UV–vis absorbance spectrum with both CYP125A6 and CYP125A7 enzymes. Overall this suggests that the presence of different substitutions at the C-3 (for example, a sulfate group), changes in the position of or removal of the A/B ring double bond and the C-7 position (ketone group) can alter substrate binding (Fig. 2 and Fig. 3) [58]. Interestingly, we observed differences between the two CYP125 enzymes with several of the cholesterol analogues tested here (Table 1). For example, CYP125A6 had a preference for an α-hydroxy species at C-7 over the β-hydroxy analogue while the reverse trend was observed with CYP125A7.

Table 2
Distances between the cholest-4-en-3-one ligand of the CYP125A1 (PDB 2X5W), CYP125A6 and CYP125A7 AlphaFold models and active site amino acids [65]. Hydrophilic interactions are highlighted in bold.

cholest-4-en-3-one	CYP125A7	Distance (Å)	CYP125A6	Distance (Å)	CYP125A1	Distance (Å)
C2	$C^{\gamma 4}$-K198	3.5	-	-	-	-
C3-O	$O^{\gamma 4}$-**D92**	3.9	**$N^{\delta 5}$-Q99**	3.6	$O^{\gamma 4}$-**D108**	4.2
C3-O	$N^{\epsilon 6}$-**K198**	3.2	-	-	$C^{\gamma 4}$-D108	3.3
C3-O	$C^{\delta 5}$-K198	2.1	-	-	$N^{\epsilon 6}$-K214	5.1
C3-O	-	-	-	-	$C^{\delta 5}$-I104	4.2
C18	$C^{\gamma 4}$-V251	2.2	-	-	$C^{\gamma 4}$-V263	3.9
C18	$C^{\gamma 4}$-V247	4.8	-	-	$C^{\gamma 4}$-V267	3.7
C18	$C^{\gamma 4}$-M184	4.9	-	-	$C^{\gamma 4}$-M200	4.3
C19	$C^{\beta 3}$-S201	2.9	-	-	$S^{\beta 3}$-S217	4.3
C19	-	-	$C^{\alpha 2}$-A204	4.3	$C^{\alpha 2}$-M200	4.9
C20	$C^{\gamma 4'}$-V251	2.5	-	-	-	-
C21	$C^{\gamma 4}$-V99	3.8	$C^{\beta 3'}$-V106	3.8	$C^{\gamma 4}$-V115	3.7
C21	-	-	$C^{\gamma 4}$-V106	4.4	$C^{\alpha 2}$-M264	4.2
C25	$C^{\alpha 2}$-A252	2.7	$C^{\alpha 2}$-A259	2.9	$C^{\alpha 2}$-A268	3.8
C25	$C^{\alpha 2'}$A252	2.5	-	-	$C^{\alpha 2'}$-A268	3.7
C26	-	-	$C^{\gamma 4}$-T263	4.0	C^{4}-F316	4.0
C26	-	-	-	-	$C^{\gamma 4}$-T272	4.0
C27	-	-	$C^{\alpha 2'}$-A259	2.6	-	-

3.2. Oxidation of cholesterol and its derivatives by the CYP125 enzymes

We next measured the ability of both enzymes to catalyze the oxidation of the panel of cholesterol analogues (Table 1) to determine if each was oxidized by these enzymes. We wished to assess if the activity would correlate with the magnitude of the shift observed in the UV–vis absorbance spectrum on substrate binding. The mixed high-spin/low-spin ferric state of the CYP125A6 and CYP125A7 enzymes may result in them not being as constrained by substrate gating as other CYP enzymes are [59–62]. The catalytic oxidation of the steroids by these enzymes was supported using spinach ferredoxin and spinach ferredoxin reductase electron transfer partners a system which is known to support the activity of these enzymes [63]. After turnover reactions were completed, the samples were extracted, dried, and derivatized with BSTFA/TMSCl prior to analysis by GC-MS (Table 1, Figs. 4–7 and Figs. S4−S18).

These oxidation reactions were compared to those of cholesterol and cholest-4-en-3-one, which both undergo ω-hydroxylation by CYP125 family members, to compare the amount of product and number of metabolites generated. The oxidation reactions of cholesterol with both CYP125A6 and CYP125A7, generated one major metabolite, being assigned based on its mass spectra and identified as 26-hydroxycholesterol (Fig. 4 and Fig. S4). With cholest-4-en-3-one both enzymes generated the terminal alcohol metabolite with CYP125A7 generating a low amount of the acid further oxidation metabolite (Fig. 4).

The majority of the other cholesterol analogues tested were also substrates for both enzymes, generating oxidized metabolites. The retention time and MS data were consistent with ω-oxidation metabolites (Fig. S7). The exceptions were cholesteryl acetate, cholesta-3,5-diene, 5α-cholestane, and 5α-cholestane-3-one with neither enzyme generating any oxidized metabolites. Cholesteryl sulfate was oxidized by CYP125A6 but not by CYP125A7 even though there was evidence of binding for the latter (Fig. 5, Fig. S4 and Table 1). In contrast, 5α-cholestan-3β-ol was only oxidized by CYP125A7 and not CYP125A6 (Fig. 5).

Table 3
Distances (Å) of carbon atoms of substrate ligands from the iron in the crystal structures of CYP125A1 (PDB 2X5W) and CYP125A6 /A7 AlphaFold models.

Structure	Distances Fe-C (Å)		
CYP125A1 cholest-4-en-3-one	5.1 (C25)	4.8 (C26)	4.3 (C27)
CYP125A7 cholest-4-en-3-one	4.8 (C25)	4.6 (C26)	4.0 (C27)
CYP125A6 cholest-4-en-3-one	5.1 (C25)	4.8 (C26)	4.4 (C27)
CYP125A7 7-ketocholesterol	4.4 (C25)	4.1 (C26)	3.8 (C27)

The other cholesterol analogues, which were modified at the steroid A ring, 5β-cholestan-3α-ol, 5β-cholestan-3β-ol and cholesterol-5α,6α-epoxide, were all oxidized by CYP125A6 and CYP125A7. The alcohol metabolite was the major product. The carboxylic acid further oxidation metabolite was also observed as a minor metabolite in these reactions (Fig. 6 and Fig. S5). This was absent in the reactions with cholesterol or cholesteryl sulfate, but is observed in reactions with CYP125A7 with cholest-4-en-3-one.

Of the cholesterol analogues that were modified on the B ring at C-7, 7-ketocholesterol and 7-dehydrocholesterol were oxidized by CYP125A6 to an ω-hydroxylation metabolite (Table 1), but the amount of product generated with 7-dehydrocholesterol was significantly lower than with 7-ketocholesterol (Fig. 7 and Fig. S5). Despite the significant UV–vis absorbance spectral response of 7-dehydrocholesterol with CYP125A7, no product was generated (Fig. S5), while the level of 7-ketocholesterol metabolite generated with CYP125A7 was also significantly lower compared to the reaction with CYP125A6 (Fig. 7).

The GC-MS analysis of the oxidation reactions of 7β-hydroxycholesterol and 7α-hydroxycholesterol were more complex due to dehydration side reactions (on either or both of the A and B rings) of the substrate and the metabolites resulting in the detection of multiple peaks in the chromatogram. Analysis of the mass spectrum of the chromatogram demonstrated that both were oxidized by CYP125A6 and CYP125A7 resulting in a mixture of alcohol and some acidic metabolites with varying stages levels of dehydration (Fig. S6, Fig. S16 and S17). The highest level of product was generated with CYP125A6 and the oxidation of 7α-hydroxycholesterol (Fig. S6 and Table 1). CYP125A7 generated more metabolites with the 7β-hydroxycholesterol over 7α-hydroxycholesterol (Fig. S6).

Overall, these results show that CYP125A6 and CYP125A7 have similar activities with cholesterol, but differences were observed with the other cholesterol analogues. For both CYP enzymes the total levels of product formation and substrate consumption was generally lower for most of the cholesterol analogues when compared to cholesterol. The levels of metabolite formed did not always correlate with the UV-spectral response to substrate binding. For example, cholesteryl sulfate and 7-dehydrocholesterol were not oxidized by CYP125A7 despite the significant spectral shift they cause in the UV–vis absorbance spectrum. However, the analogues which were modified at C-3 were not oxidized. This is in agreement with the substrate binding experiments. In general, lower levels of the hydroxylated metabolites were detected in the oxidation reactions of CYP125A7 when compared to CYP125A6. Examples include, the reactions with cholest-4-en-3-one, cholesterol-5α,6α epoxide and 7-ketocholesterol. The exception was 5α-cholestan-3β-ol

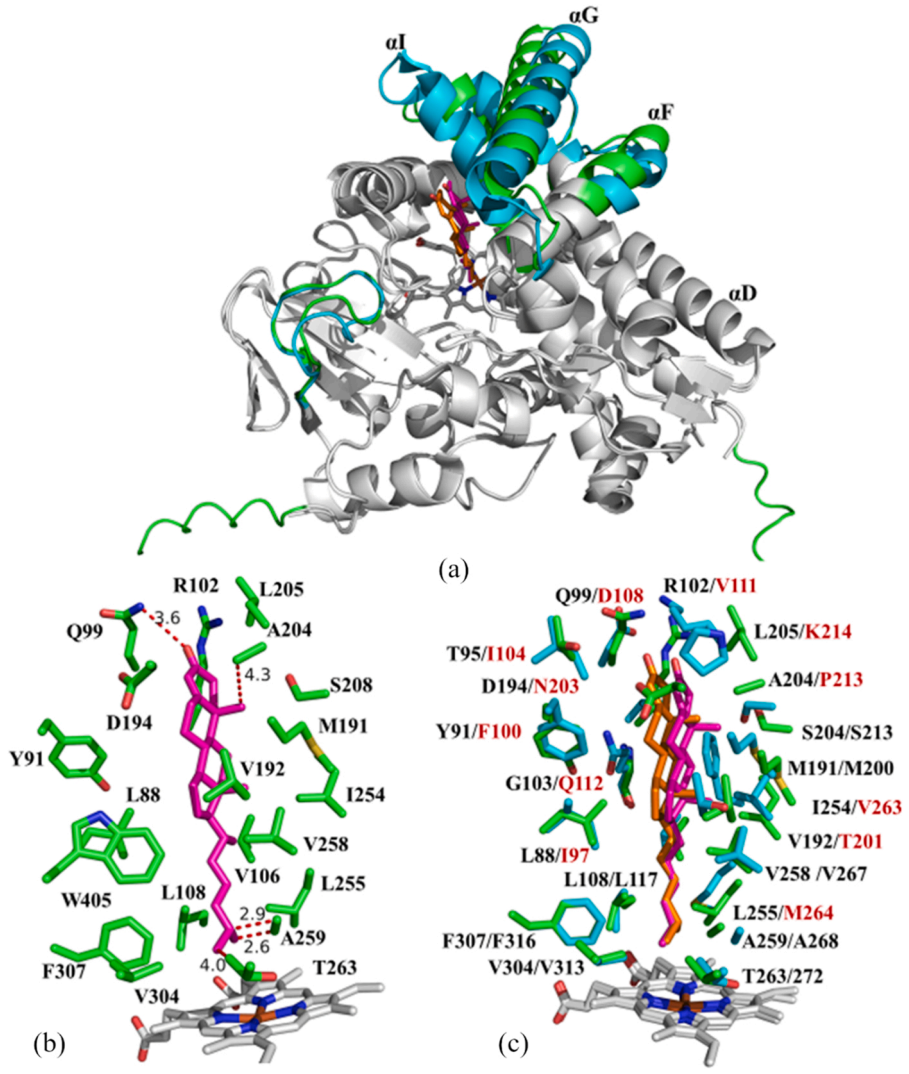

Fig. 9. (a) The superimposed structures of cholest-4-en-3-one-bound CYP125A1 (grey, highlights in teal; PDB code 2X5W) and cholest-4-en-3-one-bound CYP125A6 (grey, highlights in green; from AlphaFold). (b) The active site of the cholest-4-en-3-one-bound CYP125A6 with amino acids within 5 Å of ligand. (c) Superimposed structures of the active sites of cholest-4-en-3-one-bound CYP125A1 (teal) and cholest-4-en-3-one-bound CYP125A6 (green). The cholest-4-en-3-one substrate is shown in orange for CYP125A1 and in magenta for CYP125A6. The conserved residues in both are labelled in black and CYP125A1 residues are in red.

which yielded significantly more product with CYP125A7.

3.3. *In silico molecular docking studies*

In order to gain more insight into the function of these enzymes we examined the likely interactions between the active site residues of CYP125A7 and CYP125A6 from *M. marinum* and the cholesterol analogues. As crystal structures of these enzyme are not yet available, we used AlphaFold which employs a deep learning architecture to predict the 3D structure of a protein from its sequence [53,54]. The structure of CYP125A1 from *M. tuberculosis* with cholest-4-en-3-one has been determined by others (PDB 2X5W) [48]. To investigate the CYP125A6 and CYP125A7 enzymes we chose cholest-4-en-3-one and 7-ketocholesterol as ligands for the CYP125A7 and CYP125A6 enzymes, to analyze the active site interactions, in the vicinity of C-3 and C-7. Cholest-4-en-3-one and 7-ketocholesterol were manually docked into the binding site of the enzymes and energy minimized and annealed using ICM-Pro [64].

The overall structure of CYP125A7 from *M. marinum* was similar to that of the cholest-4-en-3-one-bound CYP125A1 structure displaying an overall RMSD value of 0.305 Å (Fig. 8a, Table S2). The largest differences were in the G-helix, F-helix, I-helix and in the F/G loop whose positions were modified relative to the CYP125A1 structure. In contrast, minimal changes in the β1-loop and the B/C-loop were observed. The active site residues that are involved in steroid binding in CYP125A7 and CYP125A1 are highly conserved. Changes are observed only at two of the active site residues: the CYP125A7 residue A197 is altered to a P213 and T187 for N203. (Fig. 8b, Fig. S20).

Analysis of the in-silico modelling studies of cholest-4-en-3-one-bound CYP125A7 AlphaFold model showed two key interactions. The C-3 ketone group of cholest-4-en-3-one interacts with the two closest amino acids at the top of the active site. The first interaction of the C-3 keto group is with the amine group of K198, and the second is with the carboxylate group of D92 (distances of 3.2 Å and 3.9 Å for K198 and D92, respectively). These two residues are close to the surface of the protein at the top of the substrate binding channel and also interact with each other (2.7 Å). This interaction closes off the substrate binding channel from the bulk solvent (Fig. 8c). For comparison, the carbonyl group at C-3 position of the cholest-4-en-3-one-bound CYP125A1 is positioned 4.1 Å and 5.1 Å away from the carboxylate group of D108 and the amine group of K214, respectively. The C-3 carbonyl oxygen also forms extra interactions with D108 and I104 in CYP125A1 (Fig. 8d).

The substrate binding pocket of CYP125A7 is defined by 21 surrounding amino acid residues all within 5 Å of the ligand (Fig. S20).

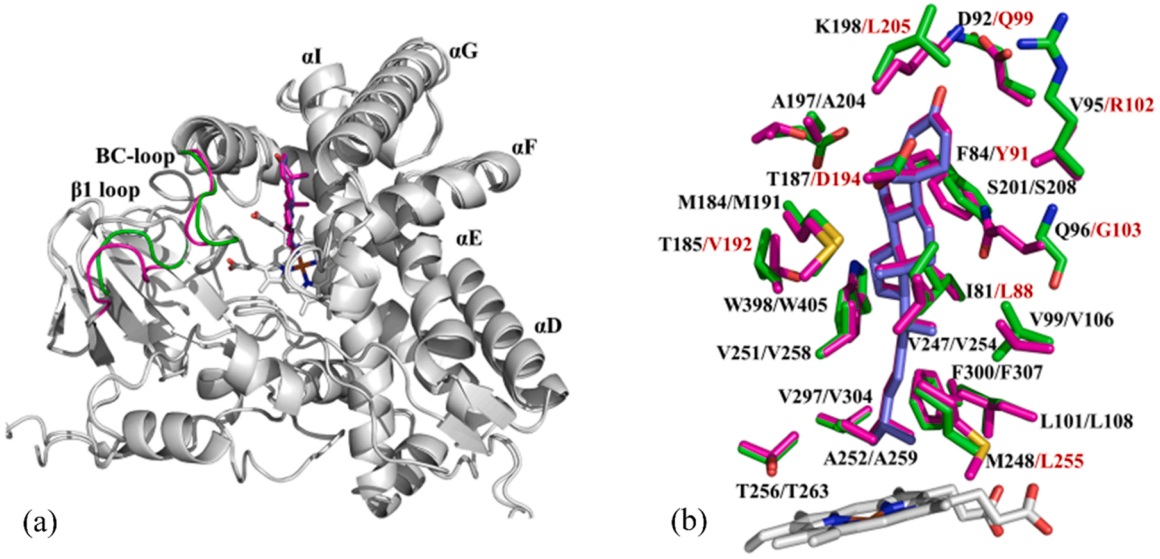

Fig. 10. (a) The superimposed structures of cholest-4-en-3-one-bound CYP125A7 (grey, highlights in magenta) and cholest-4-en-3-one-bound CYP125A6 (grey, highlights in green), using AlphaFold. (b) Superimposed structures of the active sites of cholest-4-en-3-one-bound CYP125A7 (magenta) and cholest-4-en-3-one-bound CYP125A6 (green). The cholest-4-en-3-one substrate is shown in purple for CYP125A7 and in magenta for CYP125A6. The conserved residues in both are labelled in black and CYP125A7 residues are in red.

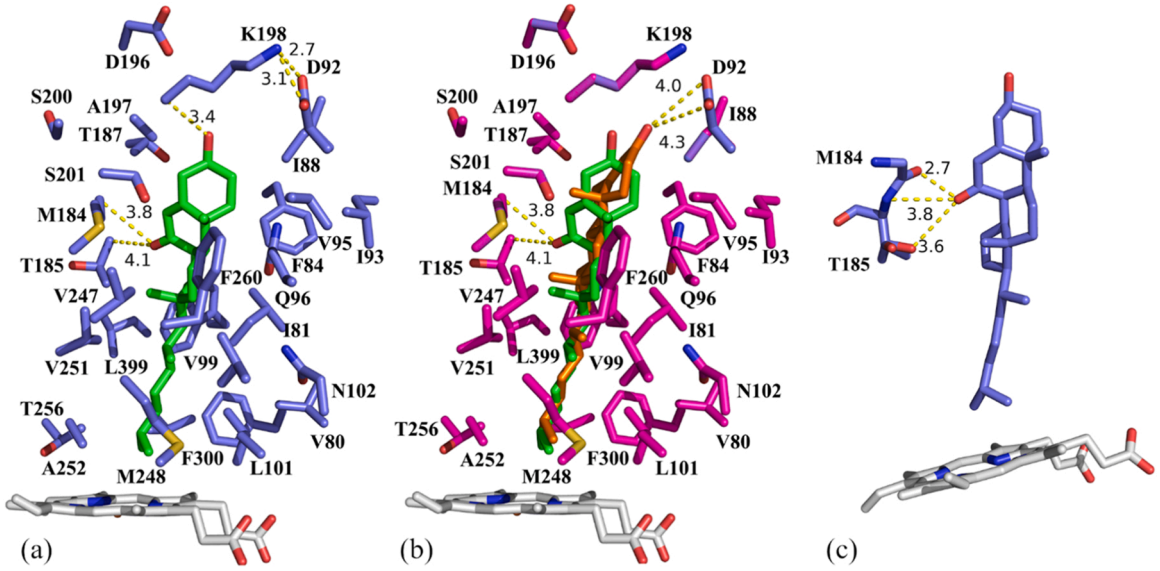

Fig. 11. (a) The docking pose of 7-ketocholesterol in the active site of CYP125A7 with amino acids within 5 Å of ligand (b) The superimposed structures of cholest-4-en-3-one-bound CYP125A7 (magenta) and 7-ketocholesterol docked in the CYP125A7 (purple). (c) The docking pose of 7-ketocholesterol in the active site of CYP125A7 with alternate conformation of the threonine 185 residue.

Amino acids within the active site, which closely interact with the cholest-4-en-3-one ligand via Van der Waals interactions are V251 with both C-18 (2.2 Å) and C-20 (2.5 Å), A252 with C-25 (2.5 Å, 2.7 Å), and K198 with C-2 (3.5 Å) (Table 2). In addition, there are other numerous Van der Waals interactions including those that are formed between the axially oriented C-18, C-19 and C-21 methyl groups within the active site that hold the cholest-4-en-3-one ligand in place. These are; S201 with C-19 (2.9 Å), V99 with C-21 (3.8 Å) (Fig. 8c and Table 2). The ω-methyl group of C-27 of cholest-4-en-3-one is 4.0 Å from the heme centre in an ideal position for C-H bond abstraction. The next closest carbons are C-25 and C-26 which are 4.8 and 4.6 Å for the iron, respectively (Table 3). The equivalent distances of the cholest-4-en-3-one-bound CYP125A1 enzyme are shown in (Table 2 and Fig. 8d).

We also compared the structures of the cholest-4-en-3-one-bound CYP125A6 AlphaFold model with cholest-4-en-3-one-bound CYP125A1 (PDB 2X5W, Fig. 9). Similar to CYP125A7 the main differences between these two structures are the related displacement of the F/G-loop and the F, G and I helices (Fig. 9a). The active site residues that are involved in steroid binding in CYP125A6 and CYP125A1 show a higher degree of variation. There are only 4 conserved residues which are; S204/S213, M191/M200, V258/V267 and A259/268 (highlighted in black Fig. 9c). The changes of the active site residues between CYP125A6 and CYP125A1 are highlighted in red (Fig. 9c).

The C-3-keto group of the substrate is surrounded by Q99, R102 and L205 (Fig. 9b). The carbonyl oxygen interacts with the amide group of Q99 which is a distance of 3.6 Å away, whereas in CYP125A7 the C-3 carbonyl interacts with the carboxylate group of D92 (Fig. 8c). Other amino acids within the active site that fix the ligand in position, include

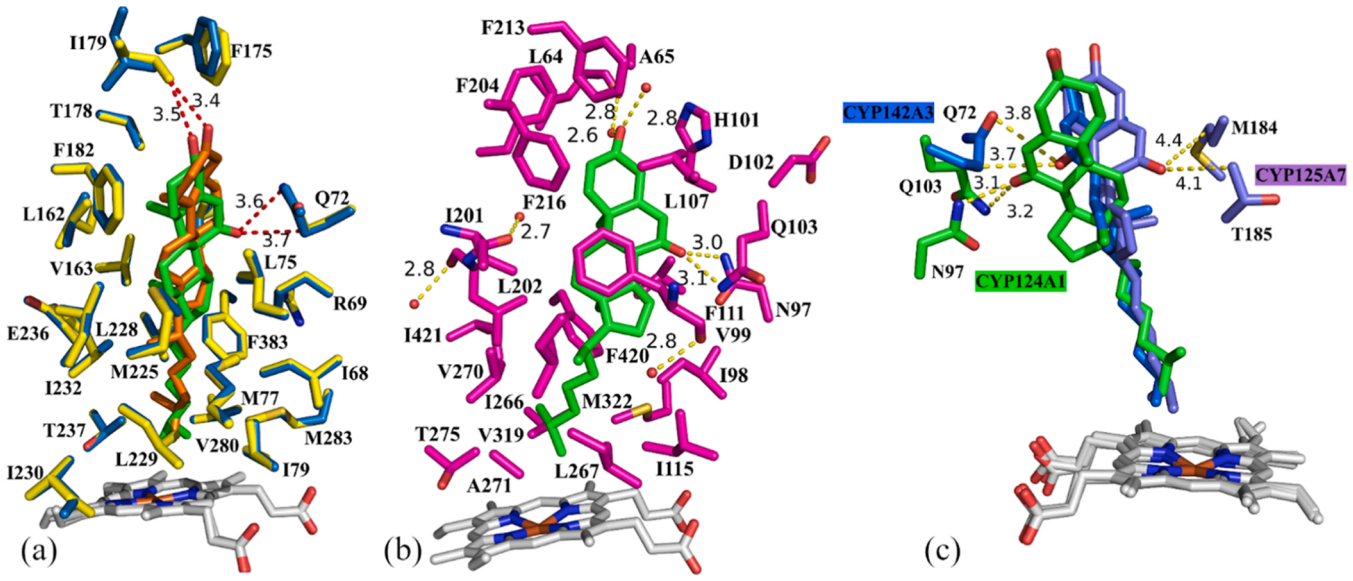

Fig. 12. (a) The superimposed structures of cholest-4-en-3-one-bound CYP142A3 (yellow; PDB code 7SMZ) and 7-ketocholesterol docked in the CYP142A3 enzyme (blue), (b) 7-ketocholesterol in the active site of CYP124A1 with amino acids within 5 Å of ligand. (c) The orientation of 7-ketocholesterol in the active site of CYP125A7, CYP142A3 and CYP124A1 from *M. marinum*, highlighting the residues interacting with C-7 keto group. For (a) and (b) The cholest-4-en-3-one substrate is shown in orange and 7-ketocholesterol in green for (c) 7-ketocholesterol in CYP124A1 is shown in green, for CYP125A7 is purple and for CYP142A3 in blue.

A204 through interactions with the axial C-19 methyl of cholest-4-en-3-one are; and V106 which interacts with C-21 (3.8 Å) [48]. The Van der Waals forces between C-25 and A268 (3.8 Å), C-26 and F316 and T272 (both 4.0 Å) and C-27 with A268 (3.7 Å) contributes to positioning the aliphatic chain in a suitable location for hydroxylation (Table 2 and Table 3). In addition, the change of P213 to A204 (Fig. 9c), which results in structural changes, appears important as it would sterically clash with the cholest-4-en-3-one ligand bound to the CYP125A6 enzyme if it did not move position.

For comparison the structures of the CYP125A6/A7 bound to cholest-4-en-3-one from AlphaFold were overlaid (Fig. 10). The overall fold of the two proteins is almost indistinguishable: there are only a minor changes in the region between helix B and B´(known as the B–C loop) and the β1 loop. This resulted in shifts in the positions of the amino acids between the two structures, for example, G44/G52, N86/D93, move by 2.2, and 2.1 Å, respectively (Fig. 10).

We also investigated the binding mode of 7-ketocholesterol with CYP125A7 from *M. marinum*. Significantly, there were different orientations of the A and B rings of the 7-ketocholesterol and the cholest-4-en-3-one ligands within the active site of the CYP125A7 enzyme (Fig. 11). The C-3 hydroxyl group of 7-ketocholesterol is located close to the top of the active site of CYP125A7 and it interacts with the K198 residue which is 3.4 Å away (Fig. 11a). This is different to the cholest-4-en-3-one-carbonyl group at C-3 in CYP125A7 which interacts with the carboxylate group of D92 (4.0 Å) (Fig. 11b). The orientation of the 7-ketocholesterol in the active site of the modelled structure of CYP125A7 places the C-7 keto group point towards T185 and M184 residues (3.8 Å and 4.1 Å from the closest atoms of M184 and T185, respectively Fig. 11a). These residues could easily alter the positions to interact favourably with the 7-keto carbonyl moiety of the substrate (Fig. 11c).

Based on a sequence alignment (Fig. S1 and Table S1), we observed that M184 in CYP125A7 is conserved in both CYP125A6 and CYP125A1 enzymes, hence similar interactions may exist between CYP125A1 (M200) and CYP125A6 (M191) and the 7-ketocholesterol ligand [39]. However, T185 in the CYP125A7 enzyme is only conserved in CYP125A1 (T201) but not in CYP125A6 (V192). We also determined that 7-ketocholesterol bound to CYP125A7 with a binding affinity (K_d, 1.7 ± 0.05 μM, Fig. S19). This is comparable to the binding affinity of this substrate with CYP124A1 (K_d, 1.1 ± 0.2 μM) and for cholest-4-en-3-one with CYP125A7 (K_d, 0.7 ± 0.4 μM) [39,66].

We and others have previously demonstrated that 7-ketocholesterol is a substrate for the CYP142 and CYP124 family member enzymes [66]. The X-ray crystal structure of 7-ketocholesterol bound to CYP124A1 (from *M. marinum,* PDB 8GDI) has also been determined [66]. To compare the binding mode of this substrate across the CYP125, CYP142 and CYP124 family members we docked the 7-ketocholesterol ligand into the active site of the cholest-4-en-3-one bound CYP142A3 enzyme from *M. marinum* (PDB 7SMZ) [50]. Similarities in the orientation of the ligands in the active site was seen (Fig. 12a). The C-3 carbonyl or hydroxyl group of the cholest-4-en-3-one and 7-ketocholesterol ligands point towards I179 at a distance of ~3.5 Å near the top of the active site. In the 7-ketocholesterol bound CYP124A1 structure the hydroxy group at C-3 interacts with two water molecules at the top of the active site which are 2.6 Å and 2.8 Å away (Fig. 12b).

These comparisons also identified differences in the binding mode and the orientation of 7-ketocholesterol in the active site of CYP124A1, CYP142A3 and CYP125A7 (Fig. 12). Fig. 12c summarizes the binding mode and the interactions of the 7-keto group with adjacent amino acids across the CYP125A7, CYP142A3, and CYP124A1 enzymes from *M. marinum*. There are notable differences across the three enzymes. In the crystal structure of 7-ketocholesterol-bound CYP124A1 the 7-keto carbonyl moiety interacts with Q103 and N97 via hydrogen bonding. In the docked structure of the CYP142A3 enzyme, the ketone of 7-ketocholesterol interacts with Q72.

3.4. Conclusions

The substrate ranges of the CYP125A6 and CYP125A7 enzymes from *M. marinum* were investigated with a set of cholesterol analogues. The CYP125A7 enzyme has a high sequence identity with CYP125A1 from *M. tuberculosis* with only a few changes within the active site amino acid residues. The trends we observe for CYP125A7 in binding and activity across cholesterol, cholest-4-en-3-one, 7-ketocholesterol and 7β-hydroxycholesterol are broadly similar to those reported by others [43]. The variations in sequence between CYP125A6 and the CYP125A7 and CYP125A1 enzymes might be expected to alter substrate recognition across these enzymes. The cholesterol analogues chosen contain substitutions at different positions on the cholesterol A and B steroid rings.

Both CYP124 and CYP142 from *M. marinum* can oxidize cholesterol, but differences in the substrate binding and levels of product formation were observed between both enzymes when substituted cholesterol analogues were studied. Despite the ability of both CYP125A6 and CYP125A7 enzymes to oxidize cholesterol, differences in the substrate binding and catalytic activity between both enzymes with different cholesterol analogues were observed. For example, while cholesteryl sulfate could bind to both enzymes it was only oxidized by CYP125A6 and not by CYP125A7.

CYP125A6 generated higher levels of metabolites with C-3 and C-7 substituted cholesterol analogues such as cholest-4-en-3-one and 7-ketocholesterol. The stereochemistry of the 5-cholestan-3-ol diastereomers resulted in differences in the binding properties and oxidation activities of these substrates across the CYP125 enzymes. Both 5α-cholestan-3β-ol and 5β-cholestan-3α-ol induced significant shifts in the Soret band with CYP125A7 but little or no spectral changes with CYP125A6. However, these substrates were still oxidized by the CYP125A6 enzyme except for 5α-cholestan-3β-ol which was only oxidized by CYP125A7 enzyme.

The CYP125A7 enzyme could accommodate cholesterol analogues with changes in the A and B rings across the C-3 to C-7 positions, for example 5β-cholestan-3β-ol and 7β-hydroxycholesterol, but in most instances generated lower levels of metabolites than CYP125A6. Neither enzyme oxidized cholesta-3,5-diene, 5α-cholestane, 5α-cholestan-3-one or cholesteryl acetate. Cholesta-3,5-diene lacks an oxygen atom at C-3, while 5α-cholestane lacks the ketone group at this position. 5α-Cholestan-3-one lacks the double bond present between C-4 and C-5 compared to cholest-4-en-3-one. Cholesteryl acetate contains a bulkier acetate group at the C-3 position. These changes in the structure of the analogues had significant adverse effects on the substrate binding and product formation with both enzymes.

Molecular modelling studies of CYP125A6 and CYP125A7 enzymes with two steroid ligands cholest-4-en-3-one and 7-ketocholesterol were also performed. This revealed differences in the binding mode of 7-ketocholesterol compared to cholest-4-en-3-one with the CYP125 enzymes with significant changes in the position of the A and B steroid rings which had rotated. There were notable differences were the interactions of the 7-keto carbonyl moiety of 7-ketocholesterol ligand with adjacent amino acids in different CYP family members. For example, in CYP125A7 this ketone points towards M184 and T185. In CYP124 interacts with Q103 and N97 via hydrogen bonding. In CYP142A3 the ketone only interacts with Q72. There were also differences in the binding mode and the orientation of 7-ketocholesterol in the active site of CYP124A1, CYP142A3 and CYP125A7.

Overall, the study of the CYP125A6 and CYP125A7 enzymes from *M. marinum* offers a further insight into the substrate range of these bacterial CYP enzymes. The analogues studied here highlight that substitutions on the substrate can change the binding position and can influence the activity. Of the other cholesterol hydroxylating CYP enzymes, the CYP142 enzyme can hydroxylate cholesterol analogues to yield the further oxidation acid metabolite in high yields [66]. With the CYP125 enzymes investigated here the alcohol metabolite was the major product, and this is more similar to CYP124A1 were also the alcohol product was more favoured [66]. CYP125A1 has been reported to catalyze C-C bond cleavage reactions of the aldehyde intermediate as an alternative to acid formation and further investigation could determine if this occurs with other CYP125 family members [48]. The CYP125 enzymes have also been demonstrated to oxidize phytosterols more efficiently than the CYP124 and CYP142 enzymes. What is required is a more complete understanding of the detailed role each of these enzymes has in the sterol catabolism pathways of bacteria.

CRediT authorship contribution statement

Amna Ghith Data curation, Methodology, Formal analysis, Investigation, Writing - Original Draft, Writing - Review & Editing, Visualization. **Stephen G. Bell** Conceptualization, methodological advice, Writing - Review & Editing, Supervision, Project administration. Funding acquisition.

Data availability

The data used is provided in the document and supplementary material. If additional data is required it is availabable on request.

Acknowledgements

This work was supported by the Australian Research Council through a Future Fellowship (FT140100355 to S.G.B.) and a Discovery project (DP210103970 to S.G.B and others). We acknowledge award of a University of Adelaide International Scholarship (PhD to A.G.).

Appendix A. Supporting information

Supplementary data associated with this article can be found in the online version at doi:10.1016/j.jsbmb.2023.106406.

References

[1] World Health Organisation, Global Tuberculosis Report 2022, https://www.who.int/teams/global-tuberculosis-programme/tb-reports/global-tuberculosis-report-2022, 2022.
[2] A. Koul, E. Arnoult, N. Lounis, J. Guillemont, K. Andries, The challenge of new drug discovery for tuberculosis, Nature 469 (2011) 483–490.
[3] A.D. Bendre, P.J. Peters, J. Kumar, Tuberculosis: Past, present and future of the treatment and drug discovery research, Current Research in Pharmacology and Drug Discovery, 2 (2021) 100037.
[4] S.T. Cole, R. Brosch, J. Parkhill, T. Garnier, C. Churcher, D. Harris, S.V. Gordon, K. Eiglmeier, S. Gas, C.E. Barry 3rd, F. Tekaia, K. Badcock, D. Basham, D. Brown, T. Chillingworth, R. Connor, R. Davies, K. Devlin, T. Feltwell, S. Gentles, N. Hamlin, S. Holroyd, T. Hornsby, K. Jagels, A. Krogh, J. McLean, S. Moule, L. Murphy, K. Oliver, J. Osborne, M.A. Quail, M.A. Rajandream, J. Rogers, S. Rutter, K. Seeger, J. Skelton, R. Squares, S. Squares, J.E. Sulston, K. Taylor, S. Whitehead, B.G. Barrell, Deciphering the biology of *Mycobacterium tuberculosis* from the complete genome sequence, Nature 393 (1998) 537–544.
[5] H. Boshoff, C. Barry III, A low-carb diet for a high-octane pathogen, Nat. Med. 11 (2005) 599–600.
[6] D.G. Russell, P.-J. Cardona, M.-J. Kim, S. Allain, F. Altare, Foamy macrophages and the progression of the human tuberculosis granuloma, Nat. Immunol. 10 (2009) 943–948.
[7] K.A. Abrahams, G.S. Besra, Mycobacterial cell wall biosynthesis: a multifaceted antibiotic target, Parasitology 145 (2018) 116–133.
[8] J.L. García, I. Uhía, B. Galán, Catabolism and biotechnological applications of cholesterol degrading bacteria, Microb. Biotechnol. 5 (2012) 679–699.
[9] M.I. Voskuil, *Mycobacterium tuberculosis* cholesterol catabolism requires a new class of acyl coenzyme A dehydrogenase, J. Bacteriol. 195 (2013) 4319–4321.
[10] H. Ouellet, J.B. Johnston, P.R.O. de Montellano, Cholesterol catabolism as a therapeutic target in *Mycobacterium tuberculosis*, Trends Microbiol. 19 (2011) 530–539.
[11] X. Yang, N.M. Nesbitt, E. Dubnau, I. Smith, N.S. Sampson, Cholesterol metabolism increases the metabolic pool of propionate in *Mycobacterium tuberculosis*, Biochemistry 48 (2009) 3819–3821.
[12] C. Demangel, T.P. Stinear, S.T. Cole, Buruli ulcer: reductive evolution enhances pathogenicity of *Mycobacterium ulcerans*, Nat. Rev. Microbiol. 7 (2009) 50–60.
[13] K. Nakanaga, R.R. Yotsu, Y. Hoshino, K. Suzuki, M. Makino, N. Ishii, Buruli ulcer and mycolactone-producing mycobacteria, Jpn. J. Infect. Dis. 66 (2013) 83–88.
[14] C.L. Daley, K.L. Winthrop, *Mycobacterium avium* complex: addressing gaps in diagnosis and management, J. Infect. Dis. 222 (2020) S199–S211.
[15] D.M. Tobin, L. Ramakrishnan, Comparative pathogenesis of *Mycobacterium marinum* and *Mycobacterium tuberculosis*, Cell. Microbiol. 10 (2008) 1027–1039.
[16] T.P. Stinear, T. Seemann, P.F. Harrison, G.A. Jenkin, J.K. Davies, P.D. Johnson, Z. Abdellah, C. Arrowsmith, T. Chillingworth, C. Churcher, Insights from the complete genome sequence of *Mycobacterium marinum* on the evolution of *Mycobacterium tuberculosis*, Genome Res. 18 (2008) 729–741.
[17] M.U. Shiloh, P.A.D. Champion, To catch a killer. What can mycobacterial models teach us about *Mycobacterium tuberculosis* pathogenesis? Curr. Opin. Microbiol. 13 (2010) 86–92.
[18] C. Cambier, S.M. Banik, J.A. Buonomo, C.R. Bertozzi, Spreading of a mycobacterial cell-surface lipid into host epithelial membranes promotes infectivity, Elife 9 (2020), e60648.
[19] T. Laval, L. Chaumont, C. Demangel, Not too fat to fight: The emerging role of macrophage fatty acid metabolism in immunity to *Mycobacterium tuberculosis*, Immunol. Rev. 301 (2021) 84–97.
[20] G. Kumar, S. Kapoor, Targeting mycobacterial membranes and membrane proteins: Progress and limitations, Bioorg. Med. Chem. 81 (2023), 117212.

[21] O.A. Trivedi, P. Arora, A. Vats, M.Z. Ansari, R. Tickoo, V. Sridharan, D. Mohanty, R.S. Gokhale, Dissecting the mechanism and assembly of a complex virulence mycobacterial lipid, Mol. Cell 17 (2005) 631–643.
[22] P.J. Brennan, Structure, function, and biogenesis of the cell wall of *Mycobacterium tuberculosis*, Tuberculosis 83 (2003) 91–97.
[23] K.Z. Rosłoniec, M.H. Wilbrink, J.K. Capyk, W.W. Mohn, M. Ostendorf, R. Van Der Geize, L. Dijkhuizen, L.D. Eltis, Cytochrome P450 125 (CYP125) catalyses C26–hydroxylation to initiate sterol side-chain degradation in *Rhodococcus jostii* RHA1, Mol. Microbiol. 74 (2009) 1031–1043.
[24] M. Parvez, L.B. Qhanya, N.T. Mthakathi, I.K. Kgosiemang, H.D. Bamal, N. S. Pagadala, T. Xie, H. Yang, H. Chen, C.W. Theron, R. Monyaki, S.C. Raselemane, V. Salewe, B.L. Mongale, R.G. Matowane, S.M. Abdalla, W.I. Booi, M. van Wyk, D. Olivier, C.E. Boucher, D.R. Nelson, J.A. Tuszynski, J.M. Blackburn, J.H. Yu, S. S. Mashele, W. Chen, K. Syed, Molecular evolutionary dynamics of cytochrome P450 monooxygenases across kingdoms: Special focus on mycobacterial P450s, Sci. Rep. 6 (2016) 33099.
[25] S. Ma, K.J. Minch, T.R. Rustad, S. Hobbs, S.-L. Zhou, D.R. Sherman, N.D. Price, Integrated modeling of gene regulatory and metabolic networks in *Mycobacterium tuberculosis*, PLoS Comput. Biol. 11 (2015), e1004543.
[26] A. Abuhammad, Cholesterol metabolism: a potential therapeutic target in Mycobacteria, Br. J. Pharmacol. 174 (2017) 2194–2208.
[27] M.D. Driscoll, K.J. McLean, C. Levy, N. Mast, I.A. Pikuleva, P. Lafite, S.E. Rigby, D. Leys, A.W. Munro, Structural and biochemical characterization of *Mycobacterium tuberculosis* CYP142: evidence for multiple cholesterol 27-hydroxylase activities in a human pathogen, J. Biol. Chem. 285 (2010) 38270–38282.
[28] J.K. Capyk, R. Kalscheuer, G.R. Stewart, J. Liu, H. Kwon, R. Zhao, S. Okamoto, W. R. Jacobs, L.D. Eltis, W.W. Mohn, Mycobacterial cytochrome P450 125 (Cyp125) catalyzes the terminal hydroxylation of C27 steroids, J. Biol. Chem. 284 (2009) 35534–35542.
[29] S. Sivaramakrishnan, H. Ouellet, H. Matsumura, S. Guan, P. Moënne-Loccoz, A. L. Burlingame, P.R. Ortiz de Montellano, Proximal ligand electron donation and reactivity of the cytochrome P450 ferric-peroxo anion, J. Am. Chem. Soc. 134 (2012) 6673–6684.
[30] A.K. Pandey, C.M. Sassetti, Mycobacterial persistence requires the utilization of host cholesterol, Proc. Natl. Acad. Sci. 105 (2008) 4376–4380.
[31] R. van Wyk, M. van Wyk, S.S. Mashele, D.R. Nelson, K. Syed, Comprehensive comparative analysis of cholesterol catabolic genes/proteins in mycobacterial species, Int. J. Mol. Sci. 20 (2019) 1032.
[32] K.J. McLean, D. Clift, D.G. Lewis, M. Sabri, P.R. Balding, M.J. Sutcliffe, D. Leys, A. W. Munro, Genomic analysis of Mtb P450 systems, Trends Microbiol. 5 (2006) 220–228.
[33] H. Ouellet, J.B. Johnston, P.R.O. de Montellano, The *Mycobacterium tuberculosis* cytochrome P450 system, Arch. Biochem. Biophys. 493 (2010) 82–95.
[34] D.A. Stahl, J. Urbance, The division between fast-and slow-growing species corresponds to natural relationships among the mycobacteria, J. Bacteriol. 172 (1990) 116–124.
[35] T. Lobastova, V. Fokina, I. Pozdnyakova-Filatova, S. Tarlachkov, A. Shutov, M. Donova, Insight into different stages of steroid degradation in thermophilic *Saccharopolyspora hirsuta* VKM Ac-666(T) Strain, Int. J. Mol. Sci. 23 (2022).
[36] K.J. McLean, J. Belcher, M.D. Driscoll, C.C. Fernandez, D. Le Van, S. Bui, M. Golovanova, A.W. Munro, The *Mycobacterium tuberculosis* cytochromes P450: physiology, biochemistry & molecular intervention, Future Med. Chem. 2 (2010) 1339–1353.
[37] J.B. Johnston, P.M. Kells, L.M. Podust, P.R. Ortiz de Montellano, Biochemical and structural characterization of CYP124: A methyl-branched lipid ω-hydroxylase from *Mycobacterium tuberculosis*, Proc. Natl. Acad. Sci. 106 (2009) 20687–20692.
[38] A. Ghith, J.B. Bruning, S.G. Bell, The catalytic activity and structure of the lipid metabolizing CYP124 cytochrome P450 enzyme from *Mycobacterium marinum*, Arch. Biochem. Biophys. (2023), 109554.
[39] S.A. Child, A. Ghith, J.B. Bruning, S.G. Bell, A comparison of steroid and lipid binding cytochrome P450s from *Mycobacterium marinum* and *Mycobacterium tuberculosis*, J. Inorg. Biochem. 209 (2020), 111116.
[40] D.J. Frank, C.A. Waddling, M. La, P.R. Ortiz de Montellano, Cytochrome P450 125A4, the third cholesterol C-26 hydroxylase from *Mycobacterium smegmatis*, Biochemistry 54 (2015) 6909–6916.
[41] D.Z. Doherty, A. Ghith, A. Ho, J.J. De Voss, S.G. Bell, The bacterial cytochrome P450 (CYP) CYP125 enzymes can competitively oxidise sitosterol in the presence of cholesterol, Chem. Commun. (2023).
[42] D.R. Nelson, L. Koymans, T. Kamataki, J.J. Stegeman, R. Feyereisen, D.J. Waxman, M.R. Waterman, O. Gotoh, M.J. Coon, R.W. Estabrook, P450 superfamily: update on new sequences, gene mapping, accession numbers and nomenclature, Pharmacogenetics 6 (1996) 1–42.
[43] T. Varaksa, S. Bukhdruker, I. Grabovec, E. Marin, A. Kavaleuski, A. Gusach, K. Kovalev, I. Maslov, A. Luginina, D. Zabelskii, R. Astashkin, M. Shevtsov, S. Smolskaya, A. Kavaleuskaya, P. Shabunya, A. Baranovsky, V. Dolgopalets, Y. Charnou, A. Savachka, R. Litvinovskaya, A. Hurski, E. Shevchenko, A. Rogachev, A. Mishin, V. Gordeliy, A. Gabrielian, D.E. Hurt, B. Nikonenko, K. Majorov, A. Apt, A. Rosenthal, A. Gilep, V. Borshchevskiy, N. Strushkevich, Metabolic fate of human immunoactive sterols in *Mycobacterium tuberculosis*, J. Mol. Biol. 433 (2021), 166763.
[44] Z.A. Zielinski, D.A. Pratt, Cholesterol autoxidation revisited: debunking the dogma associated with the most vilified of lipids, J. Am. Chem. Soc. 138 (2016) 6932–6935.
[45] W. Luu, L.J. Sharpe, I. Capell-Hattam, I.C. Gelissen, A.J. Brown, Oxysterols: old tale, new twists, Annu. Rev. Pharmacol. Toxicol. 56 (2016) 447–467.
[46] K. Prost, J.J. Birk, E. Lehndorff, R. Gerlach, W. Amelung, Steroid biomarkers revisited - improved source identification of faecal remains in archaeological soil material, PLoS One 12 (2017), e0164882.
[47] E. Jardé, G. Gruau, L. Mansuy-Huault, P. Peu, J. Martinez, Using sterols to detect pig slurry contribution to soil organic matter, Water Air Soil Pollut. 178 (2007) 169–178.
[48] H. Ouellet, S. Guan, J.B. Johnston, E.D. Chow, P.M. Kells, A.L. Burlingame, J. S. Cox, L.M. Podust, P.R.O. De, Montellano, *Mycobacterium tuberculosis* CYP125A1, a steroid C27 monooxygenase that detoxifies intracellularly generated cholest-4–en-3–one, Mol. Microbiol. 77 (2010) 730–742.
[49] S.A. Child, J.M. Bradley, T.L. Pukala, D.A. Svistunenko, N.E. Le Brun, S.G. Bell, Electron transfer ferredoxins with unusual cluster binding motifs support secondary metabolism in many bacteria, Chem. Sci. 9 (2018) 7948–7957.
[50] A. Ghith, D.Z. Doherty, J.B. Bruning, R.A. Russell, J.J. De Voss, S.G. Bell, The Structures of the Steroid Binding CYP142 Cytochrome P450 Enzymes from *Mycobacterium ulcerans* and *Mycobacterium marinum*, ACS Infect. Dis. 8 (2022) 1606–1617.
[51] S. Mayhew, D. Petering, G. Palmer, G. Foust, Spectrophotometric titration of ferredoxins and Chromatium high potential iron protein with sodium dithionite, J. Biol. Chem. 244 (1969) 2830–2834.
[52] S.A. Child, E.F. Naumann, J.B. Bruning, S.G. Bell, Structural and functional characterisation of the cytochrome P450 enzyme CYP268A2 from *Mycobacterium marinum*, Biochem. J. 475 (2018) 705–722.
[53] J. Jumper, R. Evans, A. Pritzel, T. Green, M. Figurnov, O. Ronneberger, K. Tunyasuvunakool, R. Bates, A. Žídek, A. Potapenko, Highly accurate protein structure prediction with AlphaFold, Nature 596 (2021) 583–589.
[54] M. Varadi, S. Anyango, M. Deshpande, S. Nair, C. Natassia, G. Yordanova, D. Yuan, O. Stroe, G. Wood, A. Laydon, AlphaFold Protein Structure Database: massively expanding the structural coverage of protein-sequence space with high-accuracy models, Nucleic Acids Res. 50 (2022). D439-D444.
[55] M.A. Neves, M. Totrov, R. Abagyan, Docking and scoring with ICM: the benchmarking results and strategies for improvement, J. Comput. Aided Mol. Des. 26 (2012) 675–686.
[56] B.D. Bursulaya, M. Totrov, R. Abagyan, C.L. Brooks, Comparative study of several algorithms for flexible ligand docking, J. Comput. -Aided Mol. Des. 17 (2003) 755–763.
[57] K.J. McLean, P. Lafite, C. Levy, M.R. Cheesman, N. Mast, I.A. Pikuleva, D. Leys, A. W. Munro, The structure of *Mycobacterium tuberculosis* CYP125: Molecular basis for cholesterol binding in a P450 needed for host infection, J. Biol. Chem. 284 (2009) 35524–35533.
[58] D.J. Frank, Y. Madrona, P.R.O. de Montellano, Cholesterol ester oxidation by mycobacterial cytochrome P450, J. Biol. Chem. 289 (2014) 30417–30425.
[59] M.J. Honeychurch, A.O. Hill, L.L. Wong, The thermodynamics and kinetics of electron transfer in the cytochrome P450cam enzyme system, Fed. Eur. Biochem. Soc. Lett. 451 (1999) 351–353.
[60] M.T. Fisher, S.G. Sligar, Control of heme protein redox potential and reduction rate: linear free energy relation between potential and ferric spin state equilibrium, J. Am. Chem. Soc. 107 (1985) 5018–5019.
[61] S.G. Bell, F. Xu, E.O. Johnson, I.M. Forward, M. Bartlam, Z. Rao, L.L. Wong, Protein recognition in ferredoxin-P450 electron transfer in the class I CYP199A2 system from *Rhodopseudomonas palustris*, J. Biol. Inorg. Chem. 15 (2010) 315–328.
[62] C.J. Whitehouse, S.G. Bell, W. Yang, J.A. Yorke, C.F. Blanford, A.J. Strong, E. J. Morse, M. Bartlam, Z. Rao, L.L. Wong, A highly active single-mutation variant of P450BM3 (CYP102A1), Chembiochem 10 (2009) 1654–1656.
[63] S. Ortega Ugalde, C.P. de Koning, K. Wallraven, B. Bruyneel, N.P.E. Vermeulen, T. N. Grossmann, W. Bitter, J.N.M. Commandeur, J.C. Vos, Linking cytochrome P450 enzymes from *Mycobacterium tuberculosis* to their cognate ferredoxin partners, Appl. Microbiol. Biotechnol. 102 (2018) 9231–9242.
[64] R. Abagyan, M. Totrov, D. Kuznetsov, ICM—A new method for protein modeling and design: Applications to docking and structure prediction from the distorted native conformation, J. Comput. Chem. 15 (1994) 488–506.
[65] IUPAC-IUB Joint Commission on Biochemical Nomenclature (JCBN), Nomenclature and symbolism for amino acids and peptides. Recommendations 1983, Biochem. J. 219 (1984) 345–373.
[66] A. Ghith, J.B. Bruning, S.G. Bell, The oxidation of cholesterol derivatives by the CYP124 and CYP142 enzymes from *Mycobacterium marinum*, J. Steroid Biochem. Mol. Biol. (2023), 106317.